Faculty of Engineering University of Porto

U. PORTO
FEUP **FACULDADE DE ENGENHARIA**
UNIVERSIDADE DO PORTO

Magnetic nanoparticles for cancer targeted drug delivery and imaging

Ana Isabel Ferreira Magalhães

FINAL VERSION

Dissertation performed to obtain the
Master Degree in Biomedical Engineering

Supervisor: Professor Doctor Marta Laranjeira
Co-supervisor: Professor Doctor Fernando Jorge Monteiro

Porto, June, 2018

A Dissertação intitulada

"Magnetic Nanoparticles for Cancer Targeted Drug Delivery and Imaging"

foi aprovada em provas realizadas em 05-07-2018

o júri

Presidente Prof. Doutor Jorge Alves da Silva
Professor Auxiliar do Departamento de Engenharia Informática da FEUP - U.Porto

Doutora Marta de Sousa Laranjeira
Investigadora Pós-Doutoramento do Departamento de Engenharia Metalúrgica e de Materiais - FEUP - U. Porto

Doutor Tiago Alexandre Afonso Ferreira dos Santos
Investigador Pós-Doutoramento do Instituto de Engenharia Biomédica - INEB - U. Porto

O autor declara que a presente dissertação (ou relatório de projeto) é da sua exclusiva autoria e foi escrita sem qualquer apoio externo não explicitamente autorizado. Os resultados, ideias, parágrafos, ou outros extratos tomados de ou inspirados em trabalhos de outros autores, e demais referências bibliográficas usadas, são corretamente citados.

Autor - Ana Isabel Ferreira Magalhães

Faculdade de Engenharia da Universidade do Porto

"The process of scientific discovery is, in effect, a continual flight from wonder."

Albert Einstein

Resumo

Todos os anos, milhões de pessoas morrem de cancro em todo o mundo, sendo que o cancro da mama é o tipo de cancro mais incidente entre o sexo feminino.

A quimioterapia, é considerada o modelo de tratamento standard para o cancro da mama. Contudo, para além dos efeitos secundários que lhe são inerentes, carece de especificidade, aniquilando não só as células cancerígenas, mas também as saudáveis. De momento, já se encontram aprovadas pela FDA (Food and Drug Administration) várias classes de fármacos para tratamento do cancro da mama, de entre as quais, a classe dos inibidores da aromatase. O Exemestano é um fármaco anticancerígeno normalmente utilizado para tratar cancro da mama com recetor positivo para o estrogénio (ER$^+$) em mulheres pós-menopáusicas, após tratamento com Tamoxifen.

O objetivo principal deste projeto consiste em combinar as propriedades das nanopartículas magnéticas e de sílica mesoporosa para sintetizar, produzir, caracterizar e avaliar a sua compatibilidade celular e inferir acerca do seu potencial para serem usadas como um possível sistema de libertação para o Exemestano. Para além disso, será ainda avaliado o seu potencial para serem utilizadas em hipertermia ou possivelmente como agentes de contraste em Ressonância Magnética (MRI). Este projeto inclui ainda a produção e caracterização de nanopartículas de sílica (SiNPs), nanopartículas de sílica mesoporosa (MSNs) e nanopartículas de óxido de ferro (IONs) como passos intermédios para uma melhor compreensão dos parâmetros de síntese que devem ser considerados durante a síntese das IOMSNs, no sentido de se obterem nanopartículas com propriedades promissoras para aplicações biomédicas.

Todos os tipos de nanopartículas foram caracterizados utilizando Dynamic Light Scattering (DLS), Zeta Potential (ZP), Transmission Electron Microscopy (TEM), Fourier-transform Infrared Spectroscopy (FTIR) and X-Ray Diffraction (XRD). Os resultados obtidos demonstraram que todos os tipos de nanopartículas apresentam potencial para serem utilizados em aplicações biomédicas, tendo demonstrado uma boa resposta biológica quando testadas em fibroblastos gengivais (HGnF). Contudo, concluiu-se que alguns parâmetros de síntese devem ser ajustados, especialmente no que diz respeito à uniformização dos seus tamanhos e à sua composição química.

Relativamente às IOMSNs, concluiu-se que estas apresentam uma distribuição de tamanhos não uniforme. A presença de ferro foi avaliada através da técnica de EDS-TEM e os resultados demonstraram que este se encontra presente nas IOMSNs, ainda que em baixa percentagem atómica, o que confirma as propriedades magnéticas verificadas. A técnica

de XRD demonstrou que as nanopartículas possuem uma estrutura hexagonal típica dos materiais MCM-41. Possibilitou ainda a identificação dos planos cristalinos correspondentes à magnetite, o que significa que a mesma não oxidou a maghemite durante o processo de calcinação. A capacidade de aquecimento magnético foi testada, para avaliar a possibilidade das nanopartículas virem a ser utilizadas como agentes de hipertermia. Foi verificado que estas possuem uma boa capacidade de aquecimento, no entanto, concluiu-se que protocolo de síntese deve ser otimizado para melhoria dessas mesmas propriedades.

As IOMSNs foram testadas em fibroblastos gengivais (HGnF) e concluiu-se que a morfologia alongada, característica dos fibroblastos, não sofreu alterações significativas, após incubação com as nanopartículas.

Palavras-chave: nanopartículas de sílica, nanopartículas de sílica mesoporosa, nanopartículas de óxido de ferro, nanopartículas de óxido de ferro com sílica porosa, hipertermia, ressonância magnética

Abstract

Every year, millions of people die from cancer all over the world and breast cancer is the most incident type among women.

Chemotherapy is the standard treatment modality for breast cancer. However, apart from the side effects associated, chemotherapy lacks on specificity, since it attacks not only the cancer cells but also the healthy ones. Several anticancer drugs were already approved by FDA (Food and Drug Administration) in which the aromatase inhibitors are included. Exemestane, is an antiestrogen drug, normally used to treat ER-positive breast cancer in postmenopausal women after the treatment with Tamoxifen.

The main goal of the project was to combine the properties of magnetic nanoparticles and mesoporous silica nanoparticles to produce, characterize and evaluate the cellular compatibility of the produced nanoparticles (IOMSNs) and infer about their potential to be used as a possible drug delivery system for Exemestane. Furthermore, it was analysed their potential to be used in hyperthermia therapy and as a possible MRI contrast agent. This project also included the production and characterization of Silica Nanoparticles (SiNPs), Mesoporous Silica Nanoparticles (MSNs) and Iron Oxide Nanoparticles (IONs) as intermediate steps for a better understanding of synthesis parameters that should be considered during the synthesis of IOMSNs, to obtain nanoparticles with properties suitable for biomedical applications.

All types of nanoparticles were characterized using Dynamic Light Scattering (DLS), Zeta Potential (ZP), Transmission Electron Microscopy (TEM), Fourier-transform Infrared Spectroscopy (FTIR) and X-Ray Diffraction (XRD). The results suggested that these types of nanoparticles have great potential to be used in biomedical applications, having demonstrated a good biological response when tested with Human Gingival Fibroblasts (HGnF). Nonetheless their synthesis protocols should be optimized, specially to obtain monodispersed nanoparticles in terms of size and chemical composition.

Regarding IOMSNs, it was concluded that they have a random size distribution. The presence of iron was tested using EDS-TEM and the results demonstrated that iron is present in IOMSNs in a lower atomic percentage, confirming their magnetic properties. XRD measurements demonstrated that IOMSNs have a MCM-41-like hexagonal structure. It was also possible to identify the crystalline planes corresponding to magnetite, which means that magnetite did not oxidise to maghemite during the calcination process. The magnetic heating properties were also tested, to analyse their potential to be used as a hyperthermia agent. It was verified that they have a good heating capacity, notwithstanding the synthesis protocol should be optimized to enhance their potential to be used as a hyperthermia agent.

The biological response of HGnF to IOMSNs were also tested and the results demonstrated that the cells maintained their elongated morphology after incubation with IOMSNs.

Keywords: silica nanoparticles, mesoporous silica nanoparticles, iron oxide nanoparticles, iron oxide mesoporous silica nanoparticles, hyperthermia, magnetic resonance imaging

Acknowledgements

Contents

Figures list

Tables list

Abbreviations, Acronyms and Symbols

List of abbreviations and acronyms:

A549	*Adenocarcinomic Human Alveolar Basal Epithelial cells*
BFGF	*Basic Fibroblast Growth Factor*
CMC	*Critical Micellar Concentration*
CTAB	*Hexadecyltrimethylammonium bromide*
CT	*Computerized Tomography*
DDSs	*Drug Delivery Systems*
DLS	*Dynamic Light Scattering*
EDS	*Energy-dispersive X-ray Spectroscopy*
EPR	*Enhanced Permeability Retention Effect*
ER	*Estrogen Receptor*
FBS	*Fetal Bovine Serum*
FDA	*U.S Food and Drug Administration*
H4	*Human Neuroglioma cell line*
HEK293	*Human Embryonic Kidney 293 cells*
FTIR	*Fourier-transform Infrared Spectroscopy*
HER2	*Human Epidermal growth factor Receptor-type 2*
HGnF	*Human Gingival Fibroblasts*
IOMSNs	*Iron Oxide Mesoporous Silica Nanoparticles*
IONs	*Iron Oxide Nanoparticles*
IONS-SC	*Iron Oxide Nanoparticles dispersed in Sodium Citrate*
LHRH	*Luteinizing Hormone Releasing Hormone*
LAXRD	*Low Angle X-ray Diffraction*
MNPs	*Magnetic Nanoparticles*
MPS	*Mononuclear Phagocytic System*
MRI	*Magnetic Resonance Imaging*
MSNs	*Mesoporous Silica Nanoparticles*
PBS	*Phosphate-buffered Saline*
PDI	*Polidispersity Index*
PEG	*Polyethylene glycol*

PEO	*Polyethylene oxide*
PET	*Positron Emission Tomography*
PLLA	*Polylactic acid*
SERMs	*Selective Estrogen Receptor Modulators*
SH-SY5Y	*Human Neuroblastoma Cell line*
SiNPs	*Silica Nanoparticles*
SPIONs	*Superparamagnetic Iron Oxide Nanoparticles*
TEA	*Triethanolamine*
TEM	*Transmission Electron Microscopy*
TEOS	*Triethyl orthosilicate*
VEGF	*Vascular Endothelial Growth Factor*
WAXRD	*Wide Angle X-ray Diffraction*
WHO	*World Health Organization*
XRD	*X-ray Diffraction*
ZP	*Zeta Potential*

Chapter 1

Introduction

1.1 - Cancer: statistical data and risk factors

In 2015, 8.8 million people died from cancer and it is estimated that in the next two decades, the number of new cases will rise up by about 70%, according to WHO (World Health Organization). In fact, currently, 1 out of 6 people dies of cancer, making this disease the second main cause of death worldwide, only surpassed by cardiovascular diseases (1).

Every year, 14 million new cases are discovered. Lung, liver, colorectal, cervix, stomach and breast cancers are the most recurrent ones (1, 2).

According to the last detailed statistical data published, in Portugal, in 2014, the most frequent type of cancer was prostate cancer, in males, and breast cancer in females (Figure 1.1). Several studies were performed over the years to determine which factors are responsible for cancer emergence. It was concluded that aging, tobacco, alcohol consumption, overweight, exposure to several chemicals, diets, ionizing radiation exposure, genetic factors, sunlight, chronic inflammation and some viral and bacterial infections are the main risk factors that contribute to cancer development (2, 3).

Nevertheless, in case of reduction of the risk factors, cancer could be prevented in 30-50% of the cases. For example, the use of tobacco is responsible for 22% of deaths, and it is considered one of the risk factors that could be completely eliminated (4).

Despite all the medical discoveries and technological developments, cancer's problem is not solved yet. It is mandatory to invest in the worldwide cancer research to improve the efficacy of the treatments and the prevention methodologies to find new ways to diagnose it at earlier stages, to prevent the incidence and mortality rates that have been observed over the years worldwide (5).

Males

(a)
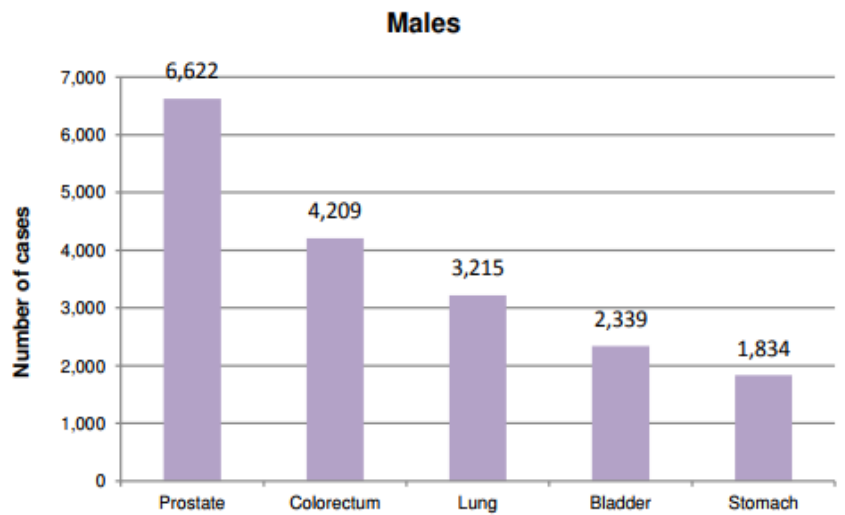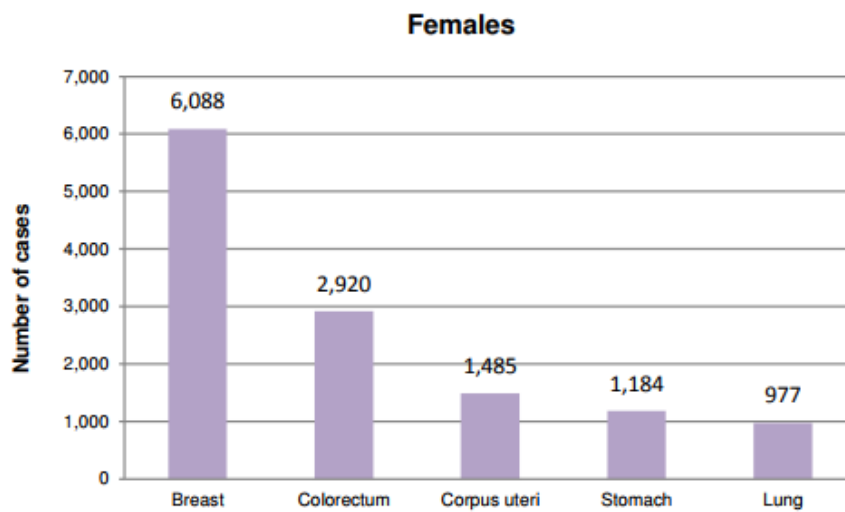
Females

(b)

Figure 1.1 - Cancer incidence in Portugal in 2014: (a) cancer incidence in males; (b) cancer incidence in females. Adapted from (2).

1.2 – The biological origin of cancer

Nowadays, cancer is considered a DNA disease. The scientific community believes that human DNA contains about 23 000 genes and around 3000 to 5000 of these genes are responsible for the production of proteins that are involved in cellular mechanisms control. When a mutation occurs in any of these genes, it is called a dysfunctional gene and the result will be an abnormal production of a certain protein, an absence of that protein production or even the production of an aberrant one. An example is the mutation that occur in a gene called KRAS. In a normal process, this gene produces a protein that makes the linking between the receptors for growth factors and the molecular signalling that sends growth signals to the nucleus to enact cellular division. If a mutation occurs in this gene, the resultant protein will become an amplifier of cell growth, generating a permanent cell division signal. As it promotes cell proliferation, it is called oncogene. On the other hand, certain genes contribute to cancer formation if they are inactivated. An example is the mutation that occur in TP53 gene. Normally, this gene produces a protein that avoids abnormal cell proliferation. When a mutation occurs in this gene, the resultant protein will be dysfunctional, and the proliferation process cannot be inhibited when it is necessary. When this happens the gene is called tumour suppressor, because it loses its function and contributes to cancer development (6).

Cancer is a result of several changes that occur in both oncogenes and tumour suppressor genes, resulting in a loss of control in cellular proliferation. The most commonly genes involved in human cancer are described below (6).

Table 1.1 - Most common oncogenes involved in human cancer. Adapted from (6).

Oncogenes	
PDGF	Codes for platelet-derived growth factor. Involved in glioma (a brain cancer).
EGFR	Codes for the receptor for epidermal growth factor. Involved in glioblastoma (a brain cancer) and breast cancer.
HER-2 or ERBB2	Codes for a growth factor receptor. Involved in breast, salivary gland and ovarian cancers.
RET	Codes for a growth factor receptor. Involved in thyroid cancer.

KRAS	Involved in lung, ovarian, colon and pancreatic cancers.
NRAS	Involved in leukemia.
MYC1	Involved in leukemia and breast, stomach and lung cancers.
NMYC	Involved in neuroblastoma (a nerve cell cancer) and glioblastoma.
LMYC	Involved in lung cancer.
BCL2	Codes for a protein that normally blocks cell suicide. Involved in follicular B cell lymphoma.
CCND1 or PRAD1	Codes for cyclin D1, a stimulatory component of the cell cycle clock. Involved in breast, head and neck cancers.
CTNB1	Codes for beta-catenin, involved in liver cancers.

Table 1.2 - Most common tumour suppressor genes involved in human cancer. Adapted from (6).

Tumor Suppressor genes	
APC	Involved in colon and stomach cancers.
DPC4	Codes for a relay molecule in a signaling pathway that inhibits cell division. Involved in pancreatic cancer.
NF-1	Codes for a protein that inhibits a stimulatory (Ras) protein. Involved in neurofibroma and pheochromocytoma (cancers of the peripheral nervous system) and myeloid leukemia.
NF-2	Involved in meningioma and ependymoma (brain cancers) and schwannoma (affecting the wrapping around peripheral nerves.
CDKN2A or MTS1	Codes for the p16 protein, a braking component of the cell cycle clock.
RB1	Codes for the pRB protein, a master brake of the cell cycle. Involved in retinoblastoma and bone, bladder, small cell lung and breast cancer.
TP53	Codes for the p53 protein, which can halt cell division and induce abnormal cells to kill themselves. Involved in a wide range of cancers.
WT1	Involved in Wilms' tumor of the kidney.
BRCA1	Involved in breast and ovarian cancers.
BRCA2	Involved in breast cancer.
VHL	Involved in renal cell cancer.

In a normal cell replication process, the human cells start to divide themselves to originate new cells. This process involves not only both cell proliferation and differentiation, but also cell death, which is necessary to maintain constant the cell number in the tissues. Cell death can occur due to exposure to certain chemicals or to a

normal programmed cell death. Programmed cell death is an active process that occurs due to series of cellular changes, in a process called apoptosis. Cell fragments and apoptotic cells are easily recognised by macrophages and neighbouring cells and they are quickly eliminated from the tissues. However, sometimes, some errors occur in cellular division giving origin to damaged cells that are not recognized by the immune system, since they can be masked and become invisible to the body. When that happens, aberrant cells start to divide themselves in an uncontrollable way, generating clones of damaged cells, forming tumours. Tumours are masses of tissue that can be either malignant or benign. A malignant tumour is the one that can invade the nearby tissues and can enter in the circulatory and lymphatic systems to spread into other parts of the body, creating metastases. On the other hand, benign tumours are the ones that are restricted to the origin local, they do not proliferate and once removed, they normally do not grow back, while malignant tumours sometimes do (7, 8).

At a cellular level, the tumour formation is viewed as a multistep process, which involves mutation and selection of cells that increase progressively their ability of proliferation, survival, metastization and invasion. The first step of tumour's formation is the tumour initiation which results from a DNA alteration, leading to an abnormal proliferation of a damaged cell. The cell proliferation gives rise to a clone of damaged cells. Additional mutations can occur during tumour progression in the population of damaged cells. Some of the mutations that may occur can bring some advantages to the mutated cells, accelerating their cell growth, and the cells that result from their cellular division will become dominant in the tumour cell population. This process is called clone selection, since a new clone of cells is formed as a consequence of the increased growth rate of the aberrant cells or a consequence of other properties, like proliferation, survival, metastization or invasion, that gave them a selective advantage. The stages of tumour development are illustrated in figure 1.2 (9).

6
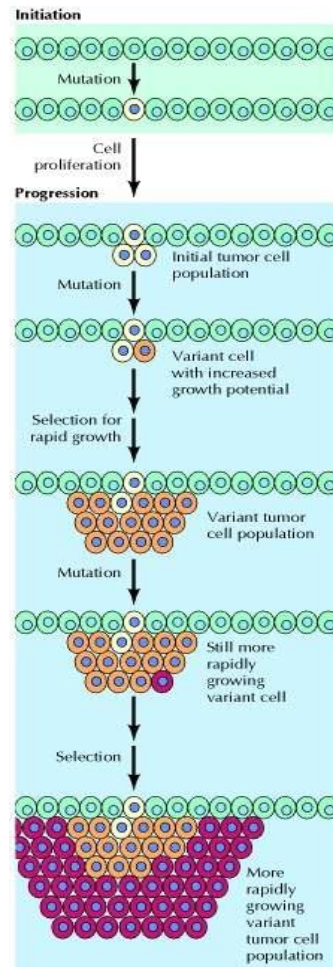
Figure 1.2 - Stages of cancer formation. Adapted from (9)

During the tumour growing process, the cancer cells can change the microenvironment in the tumour region. They need, both nutrients and oxygen supply and remove the metabolic waste and for that purpose, they induce new blood vessels formation in a process called angiogenesis. Those blood vessels are formed in response to growth factors such as vascular endothelial growth factor (VEGF), responsible for the increasing of the permeability of the blood vessels and basic fibroblast growth factor (BFGF), responsible for the recruitment of endothelial cells increasing the cell proliferation. These growth factors are secreted by tumour cells that will induce the proliferation of epithelial cells in the capillary walls, leading to the formation of new blood vessels. New blood vessels will have influence in tumour growth but also in the metastization process. Furthermore, new capillaries will promote the tumour cell proliferation since they are easily penetrated by cancer cells, allowing the metastization process (9-11).

1.2.1 - Breast cancer

According to the most recent published data, breast cancer is the most incident cancer type among women. In 2012, 1.7 million cases of female breast cancer were diagnosed across the world and 8.2 million women died as consequence of the disease. 28% of the cases were diagnosed in Europe and the mortality rate was about 25% (Figure 1.3). In Portugal, every year 6000 new cases of breast cancer are detected and around 1500 women die, according to Liga Portuguesa contra o Cancro (12-14).

The tumour heterogeneity is the main challenge to breast cancer diagnosis and treatment. The early detection of breast cancer using screening techniques can lead to the decreasing of the mortality rates. It is important to be conscious about the breast anatomy and physiology, about the diagnosis procedures and the treatments already applied for the best understanding of the disease (15, 16).

It is known that most of the therapies that have been currently applied in which chemotherapy is an example, have severe side effects for the patient since they not only clear the cancerous cells but also the healthy ones. So, it is imperative to invest in medical research to find out innovative approaches to overcome the existing failures and the side effects of the therapies that have been applied, in order to increase the survival rates and the quality of life of the patients affected (16, 17).
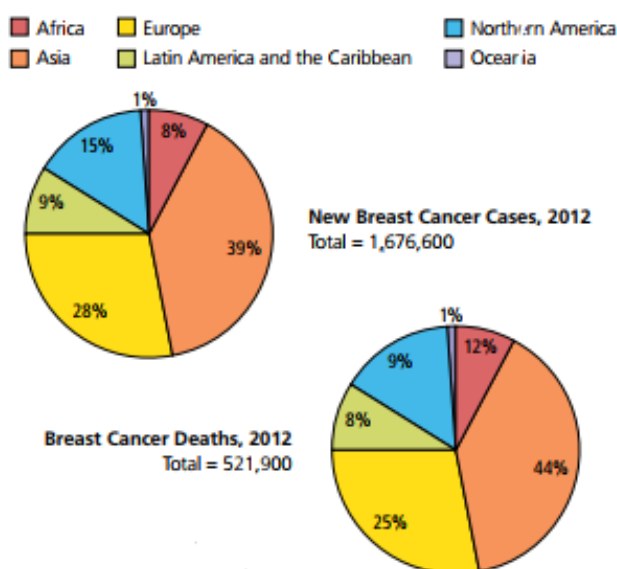
Figure 1.3 – Cancer incidence and mortality worldwide, 2012. Adapted from (5).

1.2.2 - Breast Anatomy and Physiology

Notions about the anatomy and physiology of the breast allow the best understanding of breast cancer development (Figure 1.4).

The breast is placed on top of the chest wall muscles. It is made of both glandular and fatty tissues. The glandular tissue is the responsible for milk production and it is divided in 15 to 20 sections called lobes. Each lobe gives origin to several lobules where milk is produced. Milk travels through channels called ducts which come together to form larger ducts. Larger ducts end in the nipple and the dark portion of the skin that surrounds the nipple is called areola and it contains sweet glands called Montgomery glands whose function is to secret fluids to lubricate the nipple during the breastfeeding process (18).

The fatty tissue, usually called adipose tissue, determines the size of the breast. Within the adipose tissue, there are lymph nodes, blood vessels, ligaments, lymph vessels and fibrous connective tissue (19).

The support and the shape of the breast is provided by connective tissue and ligaments and the sensation by the nerves (19).

The blood supply is done mainly by the internal mammary arteries (60%) but the thoracoacromial artery, the vessels from the serratus anterior muscle, the lateral thoracic artery and some branches of the intercostal arteries also contribute to the process (19).

The breast innervation is done by the anterolateral and anteromedial branches of the intercostal nerves from T3 to T5. The supraclavicular nerves from the cervical nervous plexus are responsible for the innervation of both lateral and upper parts of the breast. Researchers believe that the innervation of the nipple is done by the lateral cutaneous branch of the T4 nerves (19).

Around 75% of the lymphatic drainage of the breast is done via lymphatic vessels that drain into the axillary nodes. Most of the remaining drainage is done into parasternal nodes that are placed deeply to the anterior thoracic wall, associated with internal thoracic artery. Another portion of drainage is done via lymphatic vessels to the intercostal nodes, placed near the heads and necks of the ribs (19).
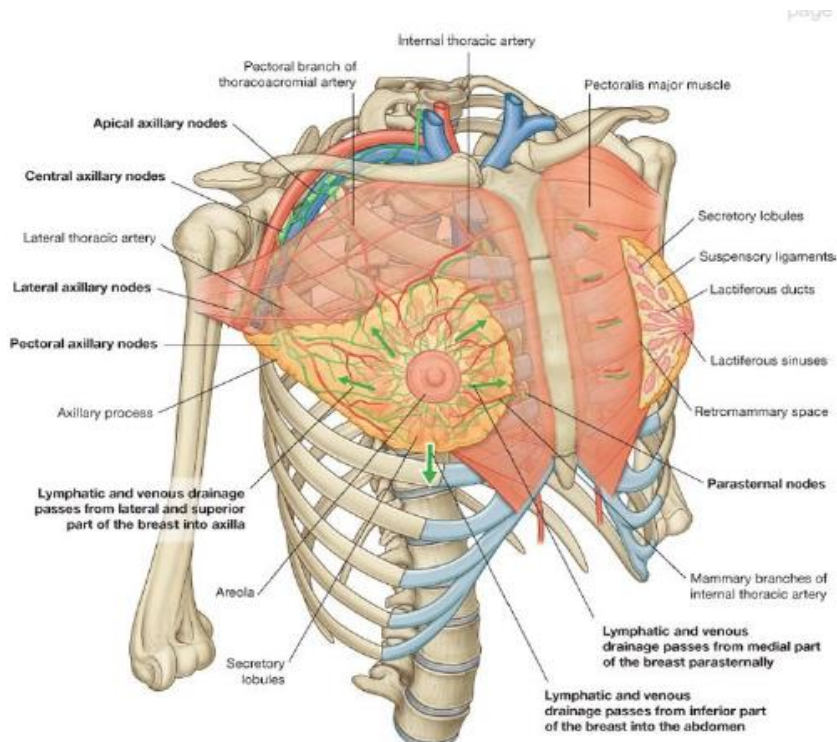
Figure 1.4 – Breast Anatomy. Adapted from (19).

1.2.3 – Types of breast cancer

A breast cancer is formed when the cells of the breast start to grow out of control and it is this uncontrollable cell division that leads to cancer development. These cells form a tumour that can be diagnosed using imaging techniques such as x-rays, mammography examinations, magnetic resonance, ultrasounds or doing a biopsy (12).

The tumour is considered malignant if it can invade the nearby tissues or metastize to other parts of the body. A benign lump results from the abnormal growth of cells but it does not proliferate to the nearby tissues. However, some benign lumps increase the probability of a woman develop breast cancer. There is an idea that the breast cancer always forms a lump and could be felt, however this is not true because some cancers, when detected in their initial stages, can only be seen in a mammography, before all the symptoms can be felt (20).

The lymphatic system is a part of the immune system and it is composed by lymph vessels connected to lymph nodes. The fluid that is carried out from the lymph vessels called lymph, contains tissue by-products, the wasting products that results from the metabolic activity of cells in the body and immune system cells. When cancer cells invade the lymph vessels, they will grow in the lymph nodes. When it occurs, there is a higher probability of the cells to spread out to other tissues of the body. That is why finding cancer cells in lymph nodes can affect the treatment plan and sometimes the affected lymph nodes are removed (18).

There are several types of breast cancers but the most common include ductal carcinoma *in situ*, invasive ductal carcinoma and invasive lobular carcinoma (17, 20)

The ductal carcinoma *in situ*, also called intraductal carcinoma is the most common type of non-invasive breast cancer. It starts in the milk ducts of the breast and it is non-invasive because it does not spread to the surrounding tissues, being placed in the original local. It is the earliest stage at which breast cancer can be diagnosed and it can be detected in 80 % of the cases using a mammogram. Despite being a non-invasive type of breast cancer, it can become invasive. The invasive ductal carcinoma differs from the ductal carcinoma *in situ* because it spreads to other parts of the body. It corresponds to 80 % of the invasive breast cancers in women and 90 % in men and the symptoms may not be felt at first. Sometimes a lump emerges in a screening mammogram which leads to testing. In some cases, it can be detected by a new lump mass formation in the breast (20, 21).

The invasive lobular carcinoma is another type of invasive breast cancer and it is the second most frequently one. It starts in the lobules of the breast, but it spreads to the nearby tissues. It is not easily detected in a medical examination, when comparing to the invasive ductal carcinoma (17, 22).

1.2.4 – Breast cancer treatment modalities

The breast cancer treatment depends on the tumour location, if it has spread to the nearby tissues and the patient health conditions. The most commonly used treatment options include surgery, radiotherapy, hormone therapy, targeted cancer drugs treatment, chemotherapy and hyperthermia (23).

The surgery can be a lumpectomy, a mastectomy with reconstruction or a surgery for lymph nodes removal. A lumpectomy is the surgery that removes the cancer area of the breast. This surgery is recommended when the tumour size is small when compared to the breast size, if the tumour is placed in a suitable position in the breast and if it is placed in only one area of the breast. A mastectomy is done when it is necessary to remove all the breast or part of it. It is an option when the tumour is large comparing to the size of the breast, when the tumour is placed in the middle of the breast or when the cancer is present in more than in one area of the breast. The surgeon can create a new breast shape using tissues from the other parts of the body or an implant. The reconstruction of the breast can occur during the mastectomy or a few months later. A modified radical mastectomy occurs when the lymph nodes present in the arm have cancer. When it happens, the surgeon removes the breast and most of or all the lymph nodes affected, since they are responsible for the lymph drainage of the breast (17, 24-26).

Radiotherapy uses X-Rays to eliminate cancer cells, it is normally done after a surgery and it decreases the chances of cancer recurrence. It is known that this type of treatment may have several side effects, but they may not affect all of the patients. Weakness, tiredness, breast changes, loss of air in the armpit and problems with arm moving are some examples of radiotherapy side effects. In a long term, the side effects may also include a swollen arm, skin changes, breathing problems, cardiac problems and bone problems (23).

The hormone therapy is applied in cancers that are affected by hormones. Hormones are produced by the body and they control the activity and the growing of the normal cells. In women, the ovaries produce estrogen and progesterone until menopause, after that, the estrogen is produced by body fat. Estrogen and progesterone are hormones that can stimulate the growth of some breast cancers, the ones in which the cells have estrogen receptors (ER). The working principle of the hormone therapy is based on the reduction of estrogen and progesterone in the body or reducing their effect, decreasing the effects of these hormones in women with ER breast cancers (23).

1 out 5 women with breast cancer has a large production of a growth promoting protein called HER2, being that cancer called HER2-positive breast cancers. This type of cancer tends to grow and spread faster that other types of breast cancers. Woman with this type of breast cancer are more likely to be successfully treated, by using drugs targeted for HER2 protein. In this case, the targeted drugs are used to stop the cell growing and proliferation, having a different action mechanism comparing to chemotherapeutic drugs, that are used to clear the cancer cells. This therapy has several side effects including heart problems, shortness of breath, leg swelling, severe fatigue and diarrhoea (27).

Chemotherapy is a technique used to treat cancer, that introduces cytotoxic drugs intravenously, to destroy the cancer cells. Not all women need chemotherapy. It is normally used before and after a surgery and in more advanced breast cancers. However, the drugs normally used can have severe side effects, affecting both cancer and healthy cells.

Hyperthermia is a cancer treatment modality in which cancer cells are exposed to temperatures higher than normal (37℃), at approximately 42 ℃. This temperature causes the cancer cells' apoptosis with minimal injury for the healthy ones. When cells are subjected to a higher increase of temperature, some changes in the cell environment start to occur. These changes make the cells more likely to be affected by either chemotherapy and radiotherapy (28-30).

The current treatment modalities have been demonstrating several limitations, specially related to their lack specificity and the severe side effects associated to the anticancer drugs administrated (31). These limitations demand new strategies capable of enhance the therapeutic effect and, at the same time, enhance the quality of life of the patients under treatment. Nanotechnology have been presenting promising approaches, that can work as an attempt to solve the problems associated with the currently applied therapies.

1.2.5 – Anticancer drugs used for breast cancer treatment

Several chemotherapeutic agents (taxanes, anthracyclines, alkylating agents, platinum drugs and vinca agents), hormone therapy agents (antiestrogen drugs, aromatase inhibitors and ovarion supressors) and targeted therapeutic agents (Afinitor ®, Avastin ®, Herceptin ®, Kadcyla ®, Tykerb ® and Perjeta ®) are already approved by FDA to be used in breast cancer management. Their mechanisms of action are described in the following tables (31).

Table 1.3 – FDA-approved Chemotherapeutic agents for breast cancer management. Adapted from (31).

Chemotherapeutic agents		
	Anticancer drugs	**Mechanism of Action**
Alkylating agents	- Cytoxan ® (cyclophosphamide) - Thiotepa I	These drugs work by inserting an alkyl agent into the DNA structure which prevents cancer cells from dividing.
Antracyclines	- Adriamycin ® (doxorubicin) - Doxil ® (liposomal doxorubicin) - Ellence (epirubicin) INovantrone ® (mitoxantrone) - Ellence (epirubicin) - Novantrone ® (mitoxantrone)	Anthracyclines are antibiotics that attack cancer cells by disrupting DNA and preventing cell division.
Platinum drugs	- Paraplatin ® (carboplatin) - Platinol ® (cisplatin)	Platinum drugs are anticancer drugs that contain the metal platinum; they bind to DNA and interfere with the cell's ability to repair itself, eventually leading to cell death.
Taxanes	- Abraxane ® (paclitaxel protein-bound) Intravenous - Taxol ® (paclitaxel) - Taxotere ® (docetaxel)	Taxanes inhibit cell growth by stopping cell division. They act by interfering with cellular microtubules, which are structures that play an important part in many cellular functions, including cell division. Taxanes are normally used combined with other chemotherapeutic agents.
Vinca agents	- Navelbine ® (vinorelbine)	Navelbine ® inhibits cancer cell growth by stopping cell division. It works by interfering with the formation of cellular microtubules, structures that help in cellular division process.

Table 1.4 - FDA-approved Hormone Therapy agents for breast cancer management. Adapted from (31).

Hormone Therapy agents		
	Anticancer drugs	**Mechanism of Action**
Anti-estrogen drugs	- Evista ® (raloxifene) - Fareston ® (toremifene) - Faslodex ® (fulvestrant) - Nolvadex ® (tamoxifen) Oral	Anti-estrogen drugs block the effects of estrogen in the breast by binding to estrogen receptors on tumor cells, by attaching themselves to receptors, anti-estrogens prevent the cell from responding to estrogen's growth-promoting activities. Raloxifene is an anti-estrogen drug approved for prevention of breast cancer by the FDA.

Aromatase inhibitors	- Arimidex (anastrozole) - Aromasin (exemestane) - Femara (letrozole)	These drugs blocks aromatase, a molecule required to produce estrogen; aromatase inhibitors are only effective in postmenopausal woman whose ovaries are no longer producing estrogen.
Ovarian suppressors	- Lupron ® (leuprolide) - Plenaxis ® (abarelix) - Suprefact ® (buserlin) - Zoladex ® (goserelin)	Suppressing the ability of the ovaries to produce estrogen is a viable treatment for estrogen-sensitive breast tumour in premenopausal women.

Table 1.5 - FDA-approved Targeted Therapy agents for breast cancer management. Adapted from (31).

Targeted Therapy agents	
Anticancer drugs	**Mechanism of Action**
Afinitor ® (everolimus)	It is a targeted therapy that acts by inhibiting an enzyme involved in cancer cell growth; everolimus specifically targets a protein kinase enzyme called mammalian target of rapamycin (mTOR).
Avastin ® (bevacizumab)	It is an ant angiogenesis targeted therapy. Antiangiogenetic therapy works by cutting off the blood supply of tumours, limiting tumour growth.
Herceptin ® (trastuzumab)	It is a monoclonal antibody that specifically attaches to the HER2 receptor, that is located on cell surface, which normally binds to a growth-promoting agent. Binding to this receptor, Herceptin ® prevents the normal growth factor from signaling the tumour cell to divide.
Kadcyla ® (T-DM1; ado-trastuzuma emtansine)	It combines Herceptin ® with a chemotherapeutic drug DM1 that interferes with cancer cell growth. Kadcyla ® delivers Herceptin ® and DM1 directly to HER2-positive cells and limits exposure of the rest of the body to the chemotherapy.
Tykerb ® (lapatinib)	It targets tumour cells that express the HER2 protein; in contrast to Herceptin ®, lapatinib blocks the HER2 protein inside the cell rather than at the cell surface.
Perjeta ® (pertuzumab)	It works by targeting a different part of the HER2 protein than Herceptin ®, resulting in further reduction in growth of HER2-protein breast cancer cells

Estrogen is a hormone that plays a key role in women physiological processes, especially in the maintenance of women sexual organs and in the female reproductive cycle. Besides that, estrogen also have influence in some diseases states, particularly in breast cancer, where it binds to specific receptors on breast cancer cells, promoting the proliferation of breast cancer cells. Most of the breast cancers have a receptor for estrogen and so they are sensitive to the

growth promoting effects of estrogen in cells. The therapies currently applied are focused on preventing the activation of the estrogen receptors by estrogens. In premenopausal women, the estrogens are produced by ovaries and estrogen's inhibition is achieved through suppression of ovarian function by surgery, ablation or by using the luteinizing hormone releasing hormone (LHRH) agonists such as gorserelin (Zoladex). However, most breast cancers occur in postmenopausal women and around 80 % of them are ER-positive, having clearly therapeutic implications. In postmenopausal women, ovaries do not produce estrogen, being the hormone produced by other non-ovarian tissues as the bone osteoblasts and chondrocytes, the vascular endothelium, the aortic smooth muscle cells, sites in the brain, skin, adipose tissue, liver, adrenal glands and also in breast tissues (32). The expression of the estrogen receptors in postmenopausal breast cancers has influence on the therapy that will be applied. Estrogen plasma levels are low in postmenopausal women when compared to the premenopausal ones however, breast tumours can be exposed to high levels of estrogens due to its production which occurs within the breast tissue itself (33).

Some years ago, it was controversial, but now it is accepted that aromatase enzyme can be found in both stromal and epithelial parts of the breast tumours. This enzyme is produced by the CYP19 gene, which is placed in cell endoplasmic reticulum and it is involved in the conversion of the C19 steroids (androgens) into C18 steroids (estrogens). Selective Estrogen Receptor Modulators (SERMs) such as Tamoxifen have been used for thirty years in clinic practices, for breast cancer treatment. Despite being well tolerated by most patients, the toxicity of Tamoxifen has raised some doubts over the years, particularly because of the associated side effects, such as vasomotor symptoms, the thromboembolism and the emergence of endometrial cancer. This fact is leading to the development of new strategies related to the suppression of estrogen production in postmenopausal women through the inhibition of the aromatase enzyme (33, 34).

Exemestane, whose commercial name is Aromasin, is an aromatase inhibitor, more specifically, it is an antiestrogen drug. It is normally used in the treatment of ER-positive breast cancer in postmenopausal women and it is normally administrated after treatment with Tamoxifen. It is well tolerated, and it has a safety profile, which are properties probably related to its mechanism of action. Exemestane binds irreversibly to the aromatase enzyme, causing its inactivation. An *in vivo* study demonstrated that the exemestane reduces the estrogen synthesis by over 97 %. As previously mentioned, estrogen has influence in the proliferation of breast cancer cells, so it is easily concluded that exemestane is a good option for the treatment of breast cancer in postmenopausal women (34). Although the oral administration of exemestane has been demonstrating to be well tolerated by patients, it may induce several side effects, including hot flashes, fatigue, nausea, increased sweating, dizziness, headache, body weight change, vaginal dryness, arthralgias, and myalgias. These problems can be solved by creating delivery systems able to provide a targeting drug delivery of exemestane into the tumour site (35).

1.3 – Nanotechnology in medicine

Novel approaches have emerged in medicine, combining multidisciplinary knowledge with technological development. Medical issues demand new therapies, diseases prevention methodologies and new treatments. Nanotechnology is a multidisciplinary area that emerged in the 80's and it develops materials, devices and systems through the manipulation of the matter at a nanometric scale, at atomic and molecular levels. The nanotechnology applications in healthcare have been increasing and they are becoming powerful tools in the replacement of traditional medical procedures presenting innovative approaches (36).

Efficient drug delivery is one of the problems that biotechnology and pharmaceutical industries have to face. Nanotechnology presents alternatives to solve the existing problems, creating nanosized platforms that work as drug delivery systems (DDS) to treat diseases like Cancer, Alzheimer and Parkinson, offering a targeted drug delivery to the disease site. In cancer therapy, DDSs play a key role in therapeutic response. Nanocarriers such as dendrimers, liposomes, polymeric and inorganic nanoparticles can be used to encapsulate anticancer drugs with low solubility presenting the following advantages: protection from metabolic degradation, enhancement of their circulation time and decrease the side effects. Nanotechnology formulates therapeutic agents within biocompatible nanoparticles that can have several compositions depending on the application for which they are developed (36-38).

1.3.1 – Nanoparticle-based drug delivery systems

In the past few decades, nanotechnology, in particularly nanoparticles, have attracted a special interest in several areas of science. Nanoparticles are solid, colloidal particles and there is no consensus in literature regarding their accepted size range, being the most common one between 10 to 1000 nm (36, 37, 39-41). Nanoparticles revolutionize the way drugs are formulated and delivered. Drugs that were previously considered unmarketable due to their low solubility, high toxicity and associated side effects can now be produced and marketed by pharmaceutical industries (37).

Conventional therapies for the treatment of cancer have been doubtful due to the poor solubility, high dosage, high toxicity, nonspecific delivery and short circulation half-lives of the anticancer drugs that have been currently administrated. Nanoparticles emerge as a solution for the anticancer drugs problems due to their advantageous properties. These nanoparticles are able to: increase the aqueous solubility of the anticancer drugs; protect them from undesirable physiological conditions; prolong their release; allow a controlled release at the target sites; improve their bioavailability; and decrease their side effects (14, 36, 37).

The effectiveness of a nanoparticle-based drug delivery system is highly dependent on particle size, since it influences its distribution, toxicity and targeting ability. As a particle becomes smaller, its surface area to volume ratio gests higher and consequently a higher

amount of the drug is closer to the particle's surface leading to a faster drug release. The size will influence the action of the lymphatic and vascular systems, the ones responsible for the clearance of the foreign substances (10, 14, 37, 41).

The surface properties are also an important aspect to take into account when a nanoparticle-based drug delivery system is designed. Frequently, the nanoparticles surface is modified to prevent the nanoparticles aggregation and clearance. A successful nanoparticle-based drug delivery system should be at the same time capable of reducing the damage caused in healthy tissues and deliver the drug to a specific tissue. In order to achieve this, it is necessary to incorporate specific targeting ligands onto the nanoparticles surface, such as peptides, nucleic acid aptamers, proteins, antibodies and small molecules. The more hydrophobic a nanoparticle surface is, the more likely is to be cleared by the immune system, because more proteins will adsorb to the particle's surface, providing a higher binding of plasma components, leading to a process called opsonization. So, it is easily concluded that turning a nanoparticle surface more hydrophilic will increase the drug blood circulation half-live. The hydrophilicity is achieved by coating the surface with polymers or surfactants or even creating copolymers like polyethylene glycol (PEG), polyethylene oxide (PEO), polyoxamer or poloxamine. PEG is a hydrophilic polymer that has been widely incorporated in nanoparticles surface, which avoids the binding of plasma proteins, making the nanoparticle surface more hydrophilic, increasing their bioavailability and reducing the opsonization problem (10, 14, 37, 41).

In addition to the size and surface properties control, the drug must be able to be released from the nanoparticle matrix. The drug release is dependent on many factors such as pH, temperature, drug solubility, drug diffusion through the matrix, desorption of the surface-absorbed or bounded drug and nanoparticle matrix swelling and erosion (37, 41).

1.3.2 – Magnetic Nanoparticles

Magnetic nanoparticles (MNPs) have been considered a powerful tool for targeting drug delivery, since they enable an extracorporeal control of internal drug release to the specific tissue under treatment. This property enhances the therapeutic efficiency since the nanoparticles can be functionalized to carry out chemotherapeutic drugs to be delivered at the tumour site, under a magnetic field application. Additionally, they can also be used in bio-imaging approaches, as contrast agents to be applied in image-guided therapies and also as hyperthermia agents (30).

To be considered a targeted drug delivery system, magnetic nanoparticles should comply with certain requirements. Nanoparticles should be monodispersed, meaning that they should have one same size range and shape. They also should be biocompatible and present a good stability, that is achieved by an inorganic or polymeric coating of the metallic core-shell structure (30). Several studies have shown the potential of magnetic nanoparticles to be used as targeted drug delivery systems. Kumar *et al*. synthesized hybrid magnetic nanoparticles with

a diameter less than 160 nm and comprising hyaluronic acid and iron oxide. They tested the ability of the nanoparticles to deliver peptides in two specific types of different cells lines, namely HEK293 (Human Enbryonic Kidney 293 cells) and A549 (Adenocarcinomic Human Alveolar Basal Epithelial cells), and the results indicated that nanoparticles delivered the peptides at about 100 %, showing a good potential to be used in cell/tissue targeting systems. Regarding the drug delivery for cancer, Jain *et al*. developed novel oleic acid-pluronic-coated iron oxide nanoparticles used to deliver high doses of anticancer drugs. Doxorubicin, a drug used in chemotherapy to treat cancer, was enclosed inside the nanoparticles and its release was tested. The nanoparticles presented a sustained drug retention and a dose-dependent antiproliferative effect on breast and prostate cancer cells (36). Hug *et al*. studied the use of PLLA coated iron oxide nanoparticles loaded with Tamoxifen, which is an anticancer drug, for targeted drug delivery. The anticancer activity was tested using MCF-7 breast cancer cell line and the results have shown that while PLLA coated iron oxide nanoparticles presented no cytotoxicity, furthermore PLLA coated iron oxide nanoparticles loaded with tamoxifen killed 80 % of the breast cancer cells after 4 days of incubation. This experiment shows the potential of PLLA coated iron oxide nanoparticles to be used as a target drug delivery system. Gunduz *et al*. used magnetic nanoparticles coated with PEG and folic acid to test the delivery of idarubicin as a target drug delivery system for breast cancer. The results showed that the conjugated nanoparticles presented higher toxicity when compared to the drug free magnetic nanoparticles, which can be an improvement for chemotherapy (30).

Besides the possibility of being used as drug delivery systems, magnetic nanoparticles can also be applied in bioimaging, as contrast agents. Bioimaging techniques include magnetic resonance imaging (MRI), computed tomography (CT), positron emission tomography (PET), optical imaging and ultrasounds (14, 30).

MRI is a non-invasive imaging technique normally used to obtain high resolution images of the internal organs as well as to obtain histological and pathological information of the living tissues under analysis, being considered one of the most powerful tools for bioimaging applications. It works based on the application of a magnetic field to a sample and normally the intensity of the applied magnetic field is 1.5 T or 3 T for clinical applications. The body has water molecules in its composition and each one of these molecules has two hydrogen protons. When a static magnetic field is applied, the water protons align according to its orientation. The strength of the magnetic field causes the water molecules to resonate at the resonance frequency. The magnetic field aligns the magnetic moments of the water protons, producing an equilibrated magnetization in the longitudinal direction. A radiofrequency pulse (RF), normally with a resonant frequency placed between 5 and 100 MHz is capable of transferring energy to the protons causing their rotation around the longitudinal axis, in phase. The angle of rotation is called flip angle. When the pulse is removed, the magnetic moment of the protons returns to the equilibrium. This process is repeated several times during the application of radiofrequency pulses and the time required for this process to occur is called relaxation time. It depends on the tissue under analysis and it can be divided into two categories: the

longitudinal relaxion (T1) and the transverse relation (T2). MRI presents high soft tissue contrast but at the same time it has a huge drawback, which is its low sensitivity. That is why it often requires the use of contrast agents. These agents are normally used to distinguish the healthy tissues from the unhealthy ones and to reduce the relaxation time of the protons. They can be divided into two classes: the ones that increase the T1 signal in T1-weighted images (usually mentioned as positive contrast agents, bright contrasts) and the T2 signal in T2-weighted images (usually mentioned as negative contrast agents, dark contrasts). T1 imaging is normally used to differentiate fat from water. In the final image it is possible to see the water with dark contrast and the fat with lighter contrast. In the T2 imaging, it is the opposite, the water is lighter, and the fat appears with darker contrast.

Core-shell nanoparticles, especially iron oxide nanoparticles (SPIONs) and ultra-small superparamagnetic nanoparticles (USPION) have been studied as possible magnetic resonance contrast agents for T2 relaxations, due to their promising properties, namely high saturation to magnetization, chemical stability, biodegradability, non-toxicity and good biocompatibility.

Iron Oxide Nanoparticles have tendency to oxidise. That is why they are normally coated with polymers like PEG, dextran and chitosan or with other coatings like silica or gold. Until now, in clinical practice, there are a few SPIONs-based systems are already implemented, and they are ferumoxsil, ferumoxides, ferucarbotran, ferristene and ferumoxsil and two more are being tested in clinical trials (30, 42-44).

Magnetic nanoparticles have been also studied due to their potential to be used as therapeutic agents in hyperthermia. Hyperthermia is a cancer treatment modality in which cancer cells are exposed to a high temperatures, normally at 42-43 ℃, without apparent damage to healthy cells (45). In 2005, DeNardo et al. thought to treat breast cancer using magnetic hyperthermia. Athymic mice bearing human breast cancer HBT 3477 xenografts were used in the study. They created a bio-probe, liking antibodies to magnetic nanoparticles and an alternating magnetic field was used to heat the probe. They studied the therapeutic and toxic responses and they found that the bio-probe could be used to provide thermoablative cancer therapy (30). Another study was perfomed in 2009 by Kikumori et al. who tested hyperthermia to treat breast cancer, using bearing mice. Anti-HER2 immunoliposomes containing magnetite (Fe_3O_4) in their constitution were synthesized and they prove that the immunoliposomes were able to generate heat under an alternating magnetic field. Liposomes were injected in tumour site and exposed to an alternating magnetic field. They found that the tumour temperature increased to 42 ℃ while the temperature of the rest of the body stayed at 38 ℃ and they also confirmed the tumour regression (30). In 2011, Chalkidou et al. tested the used of Fe-MgO nanoparticles as potential hyperthermia agents. The heating capacity of these nanoparticles were tested in vitro using different types of breast cancer cells. They concluded that nanoparticles had a fast thermal response indicating potential use for hyperthermia treatment (30).

1.3.3– Mesoporous silica nanoparticles

Mesoporous silica nanoparticles (MSNs) appeared in the mid-1990s, when Kresge and Kuroda found materials with bigger pores than zeolites, which are particles with a pore diameter of 1.5 nm. The first report on the use of MSNs as a drug delivery system was published in 2001 by Than *et al.*, and then an exponential interest started to grow regarding the use of MSNs for biomedical applications (31, 46).

MSNs have several properties that allow their use as targeted drug delivery systems. Their size and shape are easily tunable, their surface area and high pore volume give them high drug load capacity, which is very important during drug administration and blood circulation. Also, the porosity, morphology, surface charge, easy surface functionalization, high drug load capacity, high chemical stability, non-toxic behaviour and the biocompatible properties make MSNs-based systems promising drug carriers, for diagnostic catalysis, separation and sensing (46, 47).

To be applied in clinical practices, MSNs properties should be manipulated, since they may influence certain parameters that will determine the success of their application, such as biodistribution, biodegradation, drug loading and release, toxicity, bioavailability and cell uptake (46).

The MSNs biodegradation rate influences their bioavailability and the nanoparticles elimination from the body. When it is not controlled, it may cause critical side effects due to the release of certain particle components, when the particles are in their free form in circulation, becoming toxic for the cells. So, it is predicted that the best option is the one guaranteeing that the surface of the particle remains unchanged until the particle reaches the specific tissue. The procedure normally applied includes the manipulation of the MSNs surface, by surface functionalization. Surface functionalization is possible due to the presence of silanol groups from silica on nanoparticles surface which are sites where several moieties can attach to the particles, allowing the nanoparticles interaction with several biomolecules, tissues and cells, enabling a controlled drug release (46).

The bioavailability, related to the circulation time should be controlled and it is highly dependent on size, biodegradation, surface functionalization and accessibility to the target tissue (46).

The MSNs toxicity depends on particles size and surface charge. The manipulation of these properties will determine the particles behaviour in biological systems, since they will influence the particles' aggregation, protein adsorption to the nanoparticles surface and intracellular particle interactions (47).

Depending on the drug properties, specially its polarity, circulation time and degradation rate, the MSNs system should be manipulated to avoid the premature release of the drug. For that purpose, some research has been done to develop means for drug release that can be triggered by external/internal stimuli or intracellular mechanisms. There are two means by which the drug can be released: covalent linking of the drug to the support matrix, that can be

cleavable or by functionalization of the outer surface with coatings. These can change their conformation by the application of an external or internal stimulus such as light, pH, enzymes, ions, magnetic field or temperature. A MSN-based system that can respond to a certain stimulus is called a stimuli-responsive system (31, 46, 48).

The drug loading is also an important parameter to consider during the design of MSNs. Due to the large pore volumes and to high surface areas of MSNs, large amounts of drug can be incorporated by adsorption to the pore walls of the nanoparticles matrix. MSNs can carry hydrophobic drugs, which is an advantage regarding other nanocarrier systems and it is only possible due to their ceramic structure that give them chemical resistance to organic solvents (47).

MSNs can be used as theragnostic systems working as multifunctional platforms for drug delivery and cancer diagnosis. Theragnostics is a nanomedicine area that combines diagnosis and treatment options simultaneously. In theragnostics regarding breast cancer, MSNs combines imaging techniques such as PET, MRI, CT or ultrasound with breast cancer therapy, since they can be multifunctionalized. Chen *et al.* studied a system where MSNs worked as an ultrasound contrast agent and MnO_2 functionalized within pores of MSNs allowed an effective MRI, since the paramagnetic high spin ions of MnO_2 were exposed. Doxorubicin was also loaded into MSNs for simultaneous therapy. In another study, ultra-small lanthanide capped MSNs for doxorubicin loading were synthesized for cancer therapy, guided by MRI (31, 38, 46).

Regarding therapeutic applications related to breast cancer, MSNs-based systems can be categorized into active and passive targeting strategies (31).

For active targeting strategies, MSNs can be functionalized with several moieties such as peptides, aptamers and antibodies which can provide an enhanced therapeutic efficiency, reducing the toxic effects. The active targeting is possible when the particle surface is functionalized with a specific ligand that allows the nanocarrier to interact with the cancer cells and internalize them with more specificity than the treatment options already implemented in clinic methodologies. Examples of ligands include polysaccharides, folic acid, vitamins, antibodies, peptides, aptamers, etc. Several studies have proved that folic-acid functionalized MSNs produce high toxicity in breast cancer cell lines. Zhang and co-workers developed a dual folate-targeted MSNs-based system with targeted and stimuli-responsive capabilities. The results indicated that the targeted MSNs had a higher accumulation in the tumour tissues when compared to the non-targeted ones. It was also proved that there was a reduction in the tumour's weight, when the targeted MSNs were compared to the free doxorubicin and with the non-targeted particles. Targeted MSNs can also avoid the anticancer drug accumulation in other organs of the body, decreasing the toxic effects. Ultimo *et al.* developed MSNs that were functionalized with double stranded RNA polyionsinic-polycytidylic acid, which can recognize the Toll-like receptor 3, enabling the apoptosis of SK-BR-3 breast cancer cells. The doxorubicin was incorporated into MSNs, increasing the efficacy of the system. Mamaeya *et al.* developed a MSNs-based system functionalized with folic acid loaded with a γ-secretase inhibitor. The system showed a higher accumulation in breast cancer cells when

compared to non-functionalized MSNs, proving to be a good option for targeting approaches (31).

In passive targeting, the success is dependent on drug's circulation time, that is why sometimes nanoparticles are coated with some polymers such as PEG, that may alter their surface properties, making them more hydrophilic, avoiding the opsonization phenomena and increasing the circulation time of the drug, as it was described in the previous sections. Furthermore, passive targeting also depends on the Enhanced Permeability Retention effect (EPR). The EPR is a phenomenon that was discovered in 1980's when Maeda and co-workers found that certain macromolecules like polymers and proteins, with a molecular weight above 40-50 kDa accumulate in the tumour site. It occurs in solid tumours, essentially due to their high vascular density, called hypervascularization and due to their poor lymphatic drainage. This effect is considered a very important feature during the design of systems to be used in cancer therapy (31, 49).

It was concluded that nanoparticles with a size below 100 nm enter cells in an easier way than the ones with bigger diameter, due to existence of fenestrations between the endothelial cells of the cancerous tissue. There are several nanoparticles' systems for passive targeting already approved including Abraxane ®, Doxil ® and Myocet ®, evidencing an improvement in the delivery of high drug doses in cancer tissues when compared to the free drug administration. Regarding breast cancer, several systems have been studied. An example is the studied presented by Zhang *et al*. that developed nanoporous silica nanoparticles with a pore diameter of 20-60 nm for the delivery of siRNA. The system demonstrated the silencing of the genes of breast cancer cells (31).

Despite being a promising approach for targeted drug delivery, MSNs-based platforms are still not implemented in clinical procedures. However, the use of silica nanoparticles for diagnosis purposes is already approved by FDA to be tested in human clinical trials. This is a crucial step for the acceptance of the use of silica nanoparticles for clinical applications and consequently it may also be an impulse to the acceptance of MSNs as targeted drug delivery systems in the future (46).

Recent researchers have demonstrated the potential of MSNs to be used in targeted drug delivery, especially in cancer theragnostic. Their promising properties make this type of nanoparticles potential approaches to be applied in intelligent medicine regarding cancer and other biomedical applications. However, it is necessary to take in consideration the physiological restrictions of the biological systems to have an effective drug delivery process.

1.3.4 – Nanoparticles clearance from the body

The *in vitro* success of a drug delivery system is highly dependent on nanoparticle-cell interactions, while in an *in vivo* approach, the main challenge is to guarantee that the nanoparticle reaches the targeted site after administration. For an *in vivo* application, DDs have to face several issues related to the immune system, the nanoparticles transport, the

system targeting efficiency, the nanoparticles toxicity, biodegradation and biodistribution and also clearance from the body (14).

The clearance of a foreign body or substance from the body may involve certain organs such as liver, spleen, kidneys and also the action of the immune and complementary systems. It is a natural process where the body can eliminate toxic components, maintaining its healthy state. Normally, these systems are involved in the clearance of pathogens like bacteria and virus, but they also have the ability to remove external particles. The clearance process is so strong that most of the nanoparticles that are administrated intravenously are eliminated in a few minutes or hours. When nanoparticles are quickly removed, the desired targeting effect is compromised. Therefore, it is necessary to control the nanoparticles properties, to guarantee their therapeutic efficiency (14).

The mononuclear phagocytic system (MPS) and renal clearance are the two main processes by which nanoparticles are eliminated from the body. MPS is a system that involves certain organs such as the liver, the spleen and the bone marrow, that have a considerable number of phagocytic cells. It is responsible for the capture and elimination of viruses and other small objects.

As described in the previous sections, the first event to occur after nanoparticles administration is opsonization. This event occurs for all the substances that enter the body, meaning that either organisms or particles will be coated with opsonins, proteins that will make them more visible for the phagocytic cells of the MPS. Opsonization can occur in a few minutes depending on the charge and hydrophobicity of the nanoparticles and experimental studies demonstrated that a charged surface is covered by proteins more quickly comparing to a neutral surface. After the nanoparticles have attached to the phagocytic cells, their internalization by cells will occur, and afterwards they will undergo enzymatic degradation (14).

After administration, small nanoparticles have to overcome the renal clearance (50). This is a passive process that involves the glomerular filtration and the tubular secretion. It occurs due to physical filtration, called dialysis, and nanoparticles are eliminated from the body through urine. It is known that nanoparticles with a size less than 5-6 nm are quickly filtered, whereas the ones which have 6 to 8 nm in size have a lower removal efficiency. Nanoparticles with a size larger than 8 nm normally cannot be removed by this type of clearance mechanism. Beyond size, nanoparticles surface charge also has influence in renal clearance. If the nanoparticles surface charge increases, more proteins will adsorb to their surface, and consequently their diameter will also increase. Furthermore, the nanoparticles charge may interact with the glomerular wall, influencing the clearance. So, it is possible to conclude that the size and the surface charge should be optimized to control renal clearance (14, 38).

The liver can remove those nanoparticles that were not removed by the renal clearance. It is constituted by Kupffer cells, that are responsible for the removal of foreign substances through phagocytosis. Hepatocytes make up 70-80 % of the liver mass and they can also process nanoparticles, having a key role in bile excretion from the body. Particles with a size ranging

from 10-200 nm are rapidly cleared by phagocytic cells and also by hepatic filtration, taking into account that the liver's fenestrations size is between 150-200 nm (14, 51).

The spleen also helps in the removal of the nanoparticles because it has a blood filtration system composed of a 200 nm reticular mesh made of interendothelial cells. Particles over 200 nm are preferably eliminated by the spleen (14, 38).

Regarding tumour regions, it is known that for nanoparticles with sizes between 70-200 nm, there is an enhanced cellular uptake. So, it is necessary to have carefully engineered nanoparticles to delay their clearance from the body and, at the same time, guarantee their tumour cells uptake, in order to have the best possible therapeutic performance (50).

1.4 – Aim and outline of the thesis

Every year, millions of people die from cancer all over the world and breast cancer is the most incident type among women.

Chemotherapy is considered the standard treatment modality for breast cancer. However, apart from the side effects that are expected for patients under this treatment, chemotherapy lacks on specificity, since it attacks not only the cancer cells but also the healthy ones.

Several anticancer drugs are already approved by FDA (Food and Drug Administration) for breast cancer treatment, in which the aromatase inhibitors are included. Exemestane, whose commercial name is Aromasin, is an antiestrogen drug normally used to treat ER-positive breast cancer in postmenopausal women, after the treatment with Tamoxifen. It presents a safety profile when administrated, but it may cause several side effects. For this reason, it is necessary to study new alternatives to increase the efficiency of the treatment using this anticancer drug. The solution can be based on nanotechnology-based platforms, since they have been presenting promising alternatives for the problems that have been observed in currently applied therapies, associating therapeutic agents to biocompatible nanocarriers.

This project main goal is to combine the properties of magnetic nanoparticles and mesoporous silica nanoparticles to produce, characterize and evaluate the cellular compatibility of the produced nanoparticles (IOMSNs) and infer about their potential to be used as a possible drug delivery system for Exemestane. Furthermore, it will be analysed their potential to be used in hyperthermia and as a possible contrast agent for MRI applications. The project will also include the production and characterization of Silica Nanoparticles (SiNPs), Mesoporous Silica Nanoparticles (MSNs) and Iron Oxide Nanoparticles (IONs) as intermediate steps for the best understanding of synthesis parameters that should be considering during the synthesis of IOMSNs.

Chapter 2

Materials and Methods

2.1 – Nanoparticle's synthesis

2.1.1 – Synthesis of Silica Nanoparticles

Silica Nanoparticles (SiNPs) were prepared using the modified Stöber method. Briefly, 5 mL of Tetraethyl orthosilicate (TEOS, 99 % Sigma-Aldrich) were added to a mixture of 3.3 mL of Ammonium Hydroxide (NH_4OH 28-30%, Sigma-Aldrich) and 47 mL of ethanol (Merck). The mixture was maintained under stirring for 24 h at room temperature. Before drying at 60 ℃, nanoparticles were centrifuged (20 min, 44 800 g, 21 ℃) and washed three times with ultrapure water (Millipore pure water system). Then, they were powdered using a pester and a mortar and stored in an excimer flask for further use. The protocol described above was adapted from the one described in (52).

2.1.2 – Synthesis of Mesoporous silica nanoparticles

Mesoporous Silica nanoparticles (MSNs) were obtained by adding 1.0 g of Hexadecyltrimethylammonium bromide (CTAB, 99 % Sigma-Aldrich) to a mixture of 500 mL of ultrapure water (Millipore pure water system) and 4 mL of NaOH 2 M (Sodium Hydroxide, Merck). The solution was heated at 80 ℃ and maintained under stirring for 30 minutes. Then, 5 mL of TEOS (99% Sigma-Aldrich) were added to the previous solution and it was stirred 2 h at 80 ℃. Nanoparticles were centrifuged three times at 1 792 g and dried overnight at 60 ℃. Then, they were calcinated at 540 ℃ 7 h to remove the surfactant template. Afterwards, they were powdered using a pester and a mortar and stored in an excimer flask for further use. The protocol above described above was adapted from the one described in (53).

2.1.3 – Synthesis of iron oxide nanoparticles

Iron oxide nanoparticles (IONs) were obtained by adding 40 mmol of iron chloride tetrahydrate $FeCl_2 \bullet 4H_2O$ (99+%, Acros Organics) and 20 mmol of iron nitrate nonahydrate $Fe(NO_3)_3 \bullet 9H_2O$ (98+ %, Acros Organics) to 470 mL of ultrapure water. The mixture was then

heated at 70 ℃ under stirring. Then, 30 mL of NH_4OH (28-30%, Sigma-Aldrich) were added and the solution was heated at 90 ℃, for 1h under stirring.

The solution was cooled until room temperature and then, hydrochloric acid (37 %) was added until the pH reached 5.5. Iron oxide nanoparticles (IONs) were separated using a magnetic plate and they were washed three times with ultrapure water. They dried overnight at room temperature and afterwards, they were powdered with a pester and a mortar and stored in an excimer flask for further use. The protocol used was adapted from the one described in (54).

2.1.4 – Synthesis of Iron Oxide Mesoporous Silica Nanoparticles

Iron oxide mesoporous silica nanoparticles (IOMSNs) were obtained via co-precipitation method. Briefly, 1.0 g of previous prepared iron oxide nanoparticles were dispersed in 90 mL of absolute deionized water. With this objective, 1.71 g of CTAB and 1.0 g of TEA (Triethanolamine, Acros Organics, +99%) were added and the solution stirred vigorously at 80 ℃ until it dissolved completely. Subsequently, 14.0 mL of TEOS were added to the previous solution and it reacted for 2 h. The brown colloidal nanoparticles were separated using a magnet, washed several times with deionized water and dried at 60 ℃ for 24 h. Then, iron oxide mesoporous silica nanoparticles were obtained after sintering at 540 ℃ for 7 h. The protocol used was adapted from the one described in (55).

2.2 – Physicochemical Characterization

2.2.1 – Size, morphology and surface charge

Transmission Electron Microscopy (TEM) was used to determine the size and the morphology of silica nanoparticles, mesoporous silica nanoparticles, iron oxide nanoparticles and iron oxide mesoporous silica nanoparticles. To prepare samples for observation, the powders were suspended in ultrapure water in a concentration of 0.04 g/L. Solutions were sonicated 40 minutes under an ultrasonic bath. For TEM analysis, 10 µL of samples were mounted on Formvar/carbon film-coated mesh nickel grids (Electron Microscopy Sciences, Hatfield, PA, USA) and left standing for 2 minutes. The liquid in excess was removed with filter paper. The visualization was carried out on a JEOL JEM 1400 at 120 kV (Tokyo, Japan). Images were digitally recorded using a CCD digital camera Orious 1100W (Tokyo, Japan). To quantify nanoparticles' dimensions, TEM images were analysed using ImageJ ® software.

Energy Dispersed Spectroscopy (EDS) associated TEM was used to analyse the chemical composition of IOMSNs. This chemical microanalysis technique was used to characterize the elemental composition of a sample, by detecting and identifying the energy of characteristic x-rays emitted when the sample was under bombardment by an electron beam (56). For EDS analysis, the samples were mounted on nickel grids and a beryllium holder (EM-21150, Jeol Ltd.) was used. An X-Max 80 mm^2 (Oxford Instruments, Bucks, England) operated at 120 kV was coupled to the microscope.

Nanoparticles' size and surface charge were quantified using a ZetaSizer Nano ZS, at 25 ℃ with a scattering angle of 173 °. This device allows the quantification of nanoparticles' size by using the Dynamic Light Scattering (DLS). During the DLS measurement, the samples are exposed to a light beam (an electromagnetic wave) and the incident light hits the particles and both beam direction and intensity change due to a process called scattering. The intensity changes over the time contain information about that random motion and can be used to determine the diffusion coefficient of the particles. The hydrodynamic size can be determined by the diffusion coefficient using the Stokes-Einstein equation $D_f = (k_B T)/(6\pi\eta R_H)$, where D_f is the diffusion coefficient, k_B the Boltzmann constant, T is the suspension's temperature, η is the viscosity of the suspension medium and R_H is the hydrodynamic radius of the particle (57). Zeta potential is a parameter that gives information about nanoparticles' surface charge by measuring the potential at the slipping plan of a colloid particle that is moving under a magnetic field. This technique reflects the potential difference between the electric double layer of the mobile particles and the layer of dispersant around the particle in the slipping plan (58). For DLS and ZP the samples were prepared the same way as they were for TEM analysis.

2.2.2 – Chemical Profile

The characteristic chemical bounds of MSNs, IOMSNs and CTAB were recorded using a Fourier Transform Infrared (FTIR) spectrometer Perkin-Elmer 2000 with a 4 cm^{-1} spectral resolution and 32 scans per sample. To perform the analysis, 2 mg of each sample were mixed with 200 mg of KBr and the discs for analysis were obtained in a uniaxial press (Grasedy Specac).

2.2.3 – Crystal phase analysis

To determine the crystallinity of mesoporous silica nanoparticles, iron oxide nanoparticles and iron oxide mesoporous silica nanoparticles, X-ray diffraction (XRD) measurements were carried out. Before the analysis, nanoparticles were sintered at 540 ℃ at a heating rate of 5º/min for 7 h. The X-Ray patterns were obtained using a PANalytical X'Pert PRO TCU 1000 diffractometer, with monochromatic Cu radiation (λ= 1.541874 Å).

2.2.4 – Magnetic heating capacity: Hyperthermia

The magnetic heating capacity of IOMSNs was measured by placing each sample in the center of a coil of a homemade device that was kindly provided by Professor Manuel Bañobre – Lopez, under an alternating magnetic field of 180 Gauss at a frequency of m= 293 kHz. The samples were analysed in a concentration of 7 mg/mL with 1% (m/v) of sodium citrate.

2.2.5 – Magnetic properties: Magnetic Resonance Imaging

MRI analysis was performed using a 3 T clinical scanner (Sigma HDXT 3T, GE Health Care, USA), with a TR= 2500 s, TE= 77.1 s and a FOV= 18.0x18.0 cm.

2.3 – Biological response

2.3.1 – Cell culture

Human Gingival Fibroblasts (HGnF) were purchased from Sciencell and cultured with α--Minimal Essential Medium (α-MEM) containing 10 % of fetal bovine serum (FBS) and 1 % of penicillin-streptomycin (100 IU/ml and 2.5 µg/ml, Gibco, UK) and amphotericin B (2.5 µg/ml, Gibco, UK), The medium was removed every day until confluence was reached and cells were used until passage 4. All the procedures involving live cells were carried out under sterile conditions inside a laminar flow chamber and the cell incubation was carried out in a humidified atmosphere of 5 % CO_2 at 37 ºC.

2.3.2 – Cell metabolic activity

To estimate the in vitro cell viability of mesoporous silica nanoparticles, iron oxide nanoparticles and iron oxide mesoporous silica nanoparticles, a Resazurin (Sigma) Assay was performed. Resazurin is a redox dye commonly used as an indicator of chemical toxicity in cultured cells. The assay is based on the ability of metabolic active cells to reduce resazurin to the fluorescent compound, resoforin. The resoforin produced as a result of resazurin bioreduction can be measured fluorometrically and it is an indicator of cell proliferation. (59)

For cell metabolic activity evaluation, 5 000 cells were seeded in each well of a 96-well plate. After 24 h, the culture medium was refreshed with the medium containing sterilized nanoparticles at a concentration of 500 µg/mL. Afterwards, cells were incubated in new culture medium and the resazurin assay was performed at 4 h and 24 h. Briefly, after previously removing the culture medium form the wells, resazurin was added in fresh medium at a final concentration of 10 % (v/v) and incubated for 4 h, at 37 ºC. Finally, 100 µL of culture medium were extracted from each sample and fluorescence was measured at λ_{ex}= 540 nm and λ_{em}= 590 nm in a microplate reader.

2.3.3 – Cell morphology

Cell morphology was only studied for the IOMSNs, after 4 h and 24 h of incubation. It was determined by staining F-Actin with Alexa Fluor ® 488 phalloidin (nvitrogen, USA) and counterstaining the nuclei with DAPI (4',6-diamidino-2-phenylindole, Merck). The culture medium was removed, and the samples were washed three times with PBS (Phosphate Buffer Solution) and then, the cells were fixed by using 3.7 % paraformaldehyde at room temperature for 15 minutes. Then, the solution was removed, and samples were washed three times with PBS and permeabilized for 30 minutes with 0.1 % (v/v) Triton X-100 and washed again with PBS. The samples were incubated with phalloidin diluted 1:400 in PBS for 30 minutes in the dark and

then they were washed three times with PBS. Cells were incubated at 37 °C with DAPI at a concentration of 0.1 μg/mL in PBS for 10 minutes and PBS washed three times. The samples were analysed in an Inverted Fluorescence Microscope.

2.3.4 – Statistical Analysis

A one-way analysis of variance, followed by a Tukey post hoc test were used to determine possible significant differences between groups and to evaluate the statistical significance of the data, it was considered $p < 0.05$. Calculations and descriptive statistics were performed using IBM SPSS Statistics 25 for Windows® and Microsoft Office Excel 2016 ®.

Chapter 3

Results and Discussion

3.1 – Physicochemical Characterization

3.1.1 – Size, morphology and zeta potential
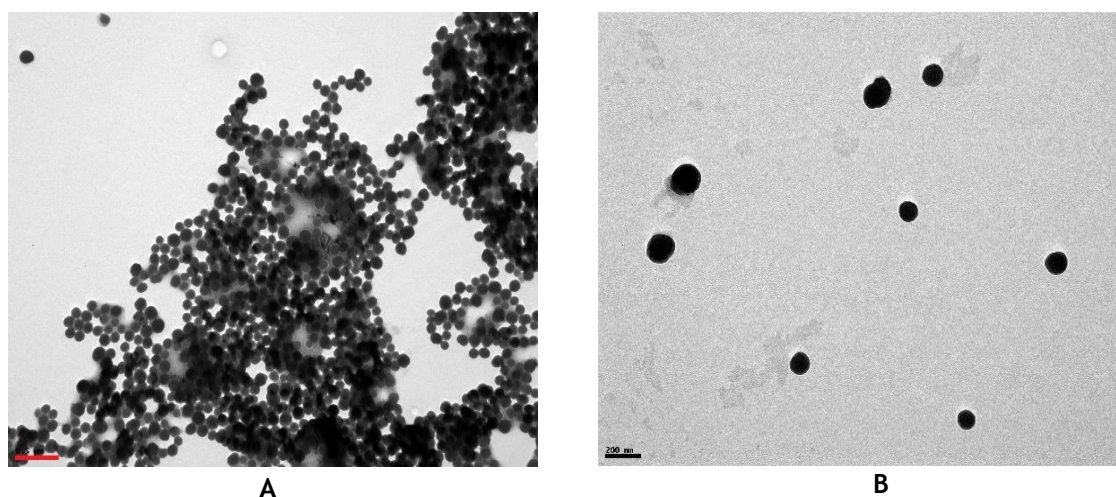
Figure 3.1 – TEM images of SiNPs (A– magnification: 25 000x scale bar: 0.5 µm; B- magnification: 50 000x, scale bar: 200 nm)
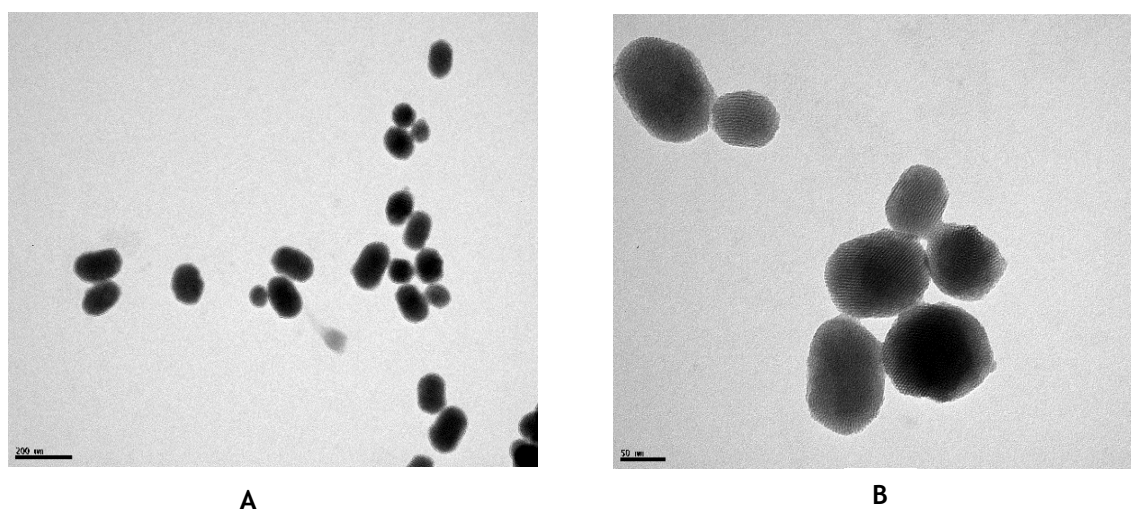
Figure 3.2 – TEM images of MSNs (A– magnification: - 80 000x scale bar: 200 nm; B- magnification: 250 000x, scale bar: 50 nm).
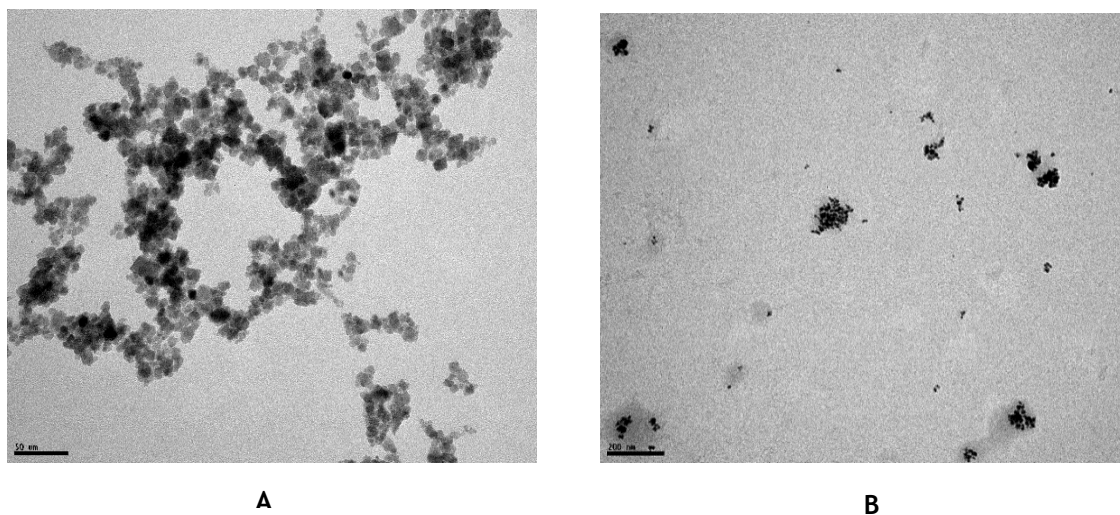
Figure 3.3 – TEM images of IONs (A), IONs dispersed using Sodium Citrate 1mM (IONs-SC-1) (B) (A–magnification: 300 000x, scale bar: 50 nm; B- magnification: 80 000x, scale bar: 200 nm).
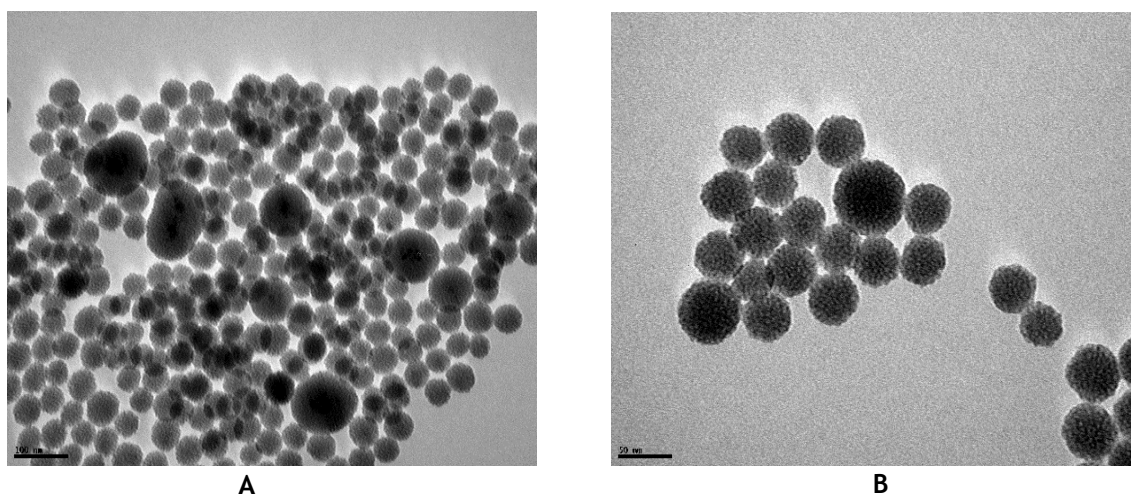
Figure 3.4 – TEM images of IOMSNs (A– magnification: 150 000x; scale bar: 100 nm; B-magnification: 300 000x; scale bar: 50 nm).

Table 3.1 – Average size (DLS and TEM) and surface charge (Zeta Potential) of SiNPs, MSNs, IONs, IOMSNs and IONs-SC-1 (d_{DLS} – average size measured using DLS; d_{TEM}- average size measured using TEM; PDI – Polydispersity Index).

		Average size (nm)		Zeta Potential (mV)
Sample	PDI	d_{DLS} (nm) (*)	d_{TEM} (nm)	
SiNPs	0.018	151.1 ± 0.4	146.3 ± 39.4	-49.1 ± 0.9
MSNs	0.381	197.4 ±15.1	151.2 ± 23.8	-16.0 ± 0.3
IONs	0.425	Aggregated	11.0 ± 1.6	-16.6 ± 0.3
IONs-SC-1	0,253	182.1 ± 30.3	143.8 ± 8.2	-30.5 ± 2.7
IOMSNs	0.611	469.6 ± 27.5	71.5 ± 37.2	-17.7 ± 0.8

(*) values obtained by the average of the intensity of the peaks

Nanoparticles' size is an important parameter for the success of their application. Different techniques may however provide different results. TEM is an excellent technique to characterize nanoparticles, since its resolution reaches about 0.07 nm, depending on the sample thickness and acceleration voltage. However, DLS is the most accurate technique to measure particle's size in nanoparticles' dispersions, allowing access not only to the particle size, but also to detect the presence of aggregates (60). The PDI value (polydispersity index), is a parameter that can be extracted by DLS data, which reflects the nanoparticles' size distribution. Samples with a wider range of particle sizes have higher PDI values and are polydispersed. On the other hand, samples with a lower range of particles' sizes have lower PDI values (lower than 0.1)(61), being monodispersed (62).

Zeta potential is normally used to characterize nanoparticles surface charge. It is known that surface charge is a parameter that as well as the size and morphology, affects the nanoparticles cellular uptake and cytotoxicity. Nanoparticles with a zeta potential between -10 mV and +10 mV are considered neutral, while those showing a zeta potential above +30 mV or less than -30 mV are considered strongly cationic and strongly anionic, respectively. Cellular membranes are negatively charged and so nanoparticles' surface charge can affect the cellular membranes, with cationic nanoparticles displaying more toxicity associated (63), since they can create pores in the cell membrane which can cause toxicity. This may happen because the pores formed can alter the concentration balance of intracellular versus extracellular ions, proteins and other important macromolecules that are required to protect the integrity and the normal function of the cell (64).

Nanoparticles' morphology, has a significant impact in cellular uptake and in nanoparticles' blood circulation, biodistribution and residency time inside the cell (65). According to this,

several studies regarding the ideal nanoparticles' morphology have been reported, however the available results generated controversy. Some studies concluded that rod-shaped nanoparticles are taken up by cells in a lower extent when compared to the spherical ones (66). Other authors concluded that rod-shaped nanoparticles have a significantly higher cellular uptake in tumour regions than the spherical ones (66). It is easily concluded that at this stage, it is not possible to take detailed conclusions regarding the nanoparticles' ideal morphology for an enhanced cellular uptake, because other parameters have influence in that process, such as the cell type, nanoparticles' size, surface charge and surface functionalization (66).

Silica nanoparticles (SiNPs) were synthesized using the modified Stöber method (52). Precipitation parameters such as concentration ratio of water and TEOS (silica precursor), reaction temperature and aging conditions can affect the SiNPs resultant particle size, morphology, distribution and agglomeration state (67). These parameters influence the nanoparticles' interactions with cells and so they have to be controlled. Based on these assumptions, different quantities of TEOS (4 mL, 5 mL, 5.5 mL and 6 mL) were tested to optimize the particle size, dispersion and morphology. It was concluded that the best results were obtained for TEOS 5 mL and that was the quantity of TEOS used in SiNPs synthesis.

The average size values of SiNPs was obtained by DLS (151.1 nm) and TEM (146.3 nm) (table 3.1). DLS measures the nanoparticles' hydrodynamic size, which comprises the nanoparticles' dimensions with interference of other molecules attached or adsorbed to nanoparticles' surface. In this case, the small differences verified between the nanoparticles' average diameters measured using TEM and DLS may be justified by the presence of water molecules adsorbed to nanoparticle surface, increasing the average size measured using DLS (60).

In the previous chapter, it was concluded that the nanoparticles' ideal size to obtain an enhanced cellular uptake in tumour regions should be found between 70 and 200 nm and SiNPs average size are within this interval. Analysing the PDI value obtained (0.018), it indicates that the sample is monodispersed, which may also be proved by looking at SiNPs TEM images (figure 3.1). TEM images also allow to identify the SiNPs spherical morphology (figure 3.1).

The zeta potential obtained for silica nanoparticles was -49.1 mV, meaning that the particles are strongly anionic. This result is lower comparing to some results already published in the literature (52) but similar to the one obtained by Shin Y. *et al*. (68). The explanation can be related to the fact that when the pH of the silica dispersion is lower than the isoelectric point of silica, the hydroxyl groups are de-protonated, producing negative charges on the surface (68). As the pH was not controlled during the synthesis of SiNPs, this can be a possible explanation for the differences verified between the zeta potential values published and the ones that were determined in this experiment.

Mesoporous Silica Nanoparticles (MSNs) were synthesized by adding TEOS to a mixture of CTAB, ultrapure water and NaOH. In the synthesis of MSNs, when the concentration of CTAB is above the Critical Micelle Concentration (CMC), CTAB self-aggregates into micelles. It is known that CTAB CMC is 1 mM and the concentration used in the synthesis of MSNs was 2 mM, which indicates the formation of micelles. When TEOS is added to the solution, it will condensate

around the polar head region of micelles, forming a silica wall around their surface. After the surfactant template removal by calcination at 540 °C for 7 h, MSNs are obtained.

As well as for SiNPs, MSNs average size were determined using DLS and TEM techniques. Comparing both average sizes, it is concluded that the average size determined using DLS (197.4 nm) was bigger when compared to the TEM ones (151.2 nm) (table 3.1). The differences between the DLS and TEM were expected and the explanation is the same as the one that was previously provided for silica nanoparticles. The values obtained for the average size are also included within the accepted interval for an enhanced cellular uptake in the tumour regions (70-200 nm), PDI was higher than 0.1 (0.381), indicating that MSNs are polydispersed. The polydispersity can also be confirmed by the TEM images (figure 3.2), since the nanoparticle random sizes are presented. It is easily concluded that the synthesis process should be optimized in order to obtain monodispersed MSNs. TEM images allowed to see the porous structure of MSNs and also their rodlike morphology. Some reports indicated that some non-spherical MSNs show advantages in biomedical applications, especially the rodlike MSNs, who had shown great potential in monitoring cell trafficking, cancer cell metastasis and drug delivery (69, 70).

The surface charge was measured using zeta potential and it was about -16.0 mV (table 3.1). This value is close to the zeta potential of MSNs whose synthesis process is similar to the one that was used in this experiment (-12.17 mV) (71). For targeted drug delivery approaches, nanoparticles surface can be functionalized to obtain the required surface charge, to have enhanced cell-nanoparticles interactions (64). This is possible due the easy surface functionalization of MSNs, due to the presence of silanol groups, which is one of the most promising features of this type of nanoparticles.

Iron Oxide Nanoparticles (IONs) were obtained by one-shot precipitation of $FeCl_2 \cdot 4H_2O$ and $Fe(NO_3)_3 \cdot 9H_2O$ with NH_4OH at 90 °C and stabilized by the addition of HCl.

As well as for SiNPs and MSNs, the average diameter of IOMSNs was determined using TEM and DLS measurements (table 3.1). Analysing the TEM results obtained for IONs, it is possible to conclude that each nanoparticle has an average size of approximately 11 nm, which is in agreement with studies already published in literature for the same type of nanoparticles (72). However, DLS measurements proved that IONs have tendency to aggregate in aqueous media, which may also be confirmed by the TEM images (figure 3.3 - A) obtained for IONs. The PDI value obtained was higher and a possible explanation can be related to the aggregation of the particles that causes a broad distribution of sizes, resulting in polydispersity (72). The aggregation process can be explained by the fact that, in the absence of a surface coating, iron oxide nanoparticles have hydrophobic surfaces with large surface areas to volume ratio. Due to hydrophobic interactions, they agglomerate and form large clusters, resulting in an increased particle size (73). The values obtained for the average size of IONs are not included in the accepted nanoparticles' size interval for an enhanced cellular uptake in the tumour regions (70-200 nm), meaning that the synthesis protocol should be optimized to prevent nanoparticles aggregation.

To overcome the aggregation problem inherent to IONs, nanoparticles are normally functionalized with surfactants, commonly with oleic acid (steric repulsion) or they may be prevented from sticking to each other by an electrostatic bilayer (electrostatic repulsion) which gives the particles stability in liquid solutions (72). Citrate ions have been also used to stabilize IONs in aqueous dispersions, providing electrostatic stabilization (74). In this experiment, a preliminary study was carried out as an attempt to disperse iron oxide nanoparticles by using sodium citrate at 1% (m/v) (IONS-SC-1). DLS measurements detected the presence of clusters of iron oxide nanoparticles with an average size of approximately 182 nm (table 3.1). Analysing the TEM results (table 3.1), it is possible to conclude that nanoparticles' clusters have an average size of approximately 143 nm. This value is similar to the average size obtained in DLS and comparing them with the average size of IONs, it is possible to predict that sodium citrate can be used as a stabilizer agent for synthesized iron oxide nanoparticles, which is proved by the lower PDI value obtained and also by TEM images (figure 3.3 – B). The average size determined is included in the average size accepted range for an enhanced cellular uptake in tumour regions.

The surface charge determined for IONs was about -16.6 mV (table 3.1). This value was obtained for a pH= 5.5 and it is known that iron oxide nanoparticles' surface charge is dependent on the pH of the solution where they are dispersed. This result is in agreement with the ones found in the literature for the same type of nanoparticles at similar pH (75). On the other hand, the surface charge determined for IONs-SC-1mM was about -30.5 mV (table 3.1), which is lower than the surface charge of IONs, proving that the citrate ions decrease the nanoparticles' surface charge, leading to an increase of nanoparticles' steric repulsion.

Although citrates have been frequently used as stabilizing agents to prevent iron oxide nanoparticles aggregation, some reported studies revealed that they may induce some cytotoxicity (76). For this reason, in this work, iron oxide nanoparticles were analysed without any dispersant or surface modification, since the main purpose was to study their physicochemical properties and potential cytotoxicity per se. However, it seems to be interesting to test the influence of different citrate concentrations in nanoparticles' dispersion as well as their cytotoxicity in future approaches.

Iron oxide mesoporous silica nanoparticles were obtained by co-precipitation by combining previous synthesized IONs with CTAB, TEA and TEOS. First, IONs were dispersed in water by ultrasonic treatment and only the stabilized particles were used for the synthesis of IOMSNs. Afterwards, CTAB and TEA were added to nanoparticles' solution. CTAB is a cationic surfactant and it acts both as structure directing agent for silica and as a stabilizer agent for iron oxide nanoparticles. TEA works like a base, as a complexing agent for silica precursor (TEOS) and as an encapsulator for mesoporous particles, thus regulating the alkoxides hydrolysis/condensation rates, limiting the particles growth and aggregation (77). TEOS is the silica precursor that will be responsible for the formation of the silica matrix.

The average sizes determined using DLS (469.6 nm) and TEM (71.5 nm) (table 3.1) are very different from each other, indicating that nanoparticles are polydispersed. This conclusion may

also be reinforced by the PDI value obtained (0.611). The results obtained for DLS measurements did not reflect the real size of the particles, because looking at the TEM images of IOMSNs (figure 3.4) it is possible to see that nanoparticles are smaller and individualized, even with a random size range.

Some reported studies defended that the molar ratio between TEA and TEOS should be controlled to tune the average nanoparticle size (78). As it was previously reported, TEA may control particles' aggregation and limit particles' size. On the other hand, the amount of TEOS may also influence particles size (79). In the synthesis protocol of IOMSNs, the amount of TEOS used is almost fourteen times higher than the amount of TEA and this proportion in much higher when compared to other protocols already published in the literature (79). This may be a justification for the random sizes and for the lower dispersion obtained. Regarding the constitution of IOMSNs, looking at the respective TEM images, it is possible to note the presence of nanoparticles with a dark core inside which may be related to iron oxide nanoparticles. However, it is not possible to observe it in all the particles and this may be justified by the fact that only the IONs stabilized with ultrasonic treatment were used in the synthesis of IOMSNs, being the amount of IONs used in the synthesis, lower than the indicated in the synthesis protocol, compared to the amount of TEOS used.

IOMSNs has a surface charge of -17.7 mV. This value traduces the lower repulsive forces between the particles, being a possible explanation for the average size obtained in DLS measurements, since the particles are close to each other.

38
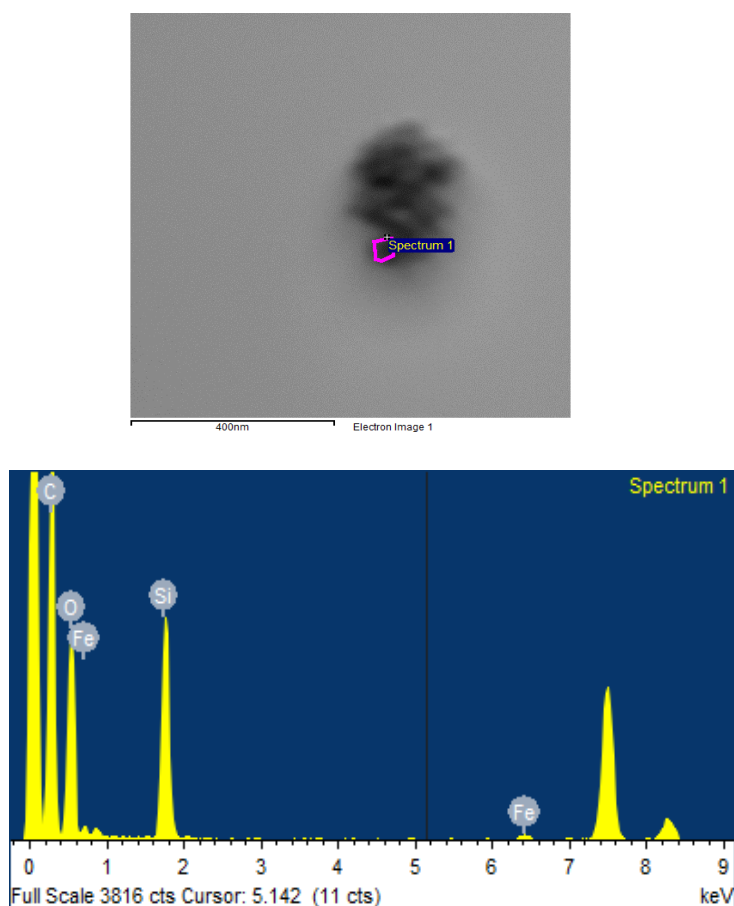
Figure 3.5 – EDS-TEM of IOMSNs.

Table 3.2 – TEM-EDS composition analysis of IOMSNs.

Element	Atomic %
C	68.62
O	21.96
Si	9.20
Fe	0.22

Energy Dispersive Spectroscopy (EDS) from TEM was used to analyse IOMSNs chemical composition, specially to prove the presence of iron in IOMSNs. The presences of carbon (C), oxygen (O), Silicon (Si) and Iron (Fe) were detected. The presence of carbon is attributed to the formvar coated grid used to analyse the sample, oxygen is probably due to the presence of SiO_2 and iron oxide, silicon is probably due to SiO_2 and the presence of iron may be due to the iron oxide.

The analysis allowed to see that iron is present in the chemical composition of IOMSNs, although in lower amounts. This result confirmed what was observed during the washing process of IOMSNs, in which a magnetic plate was used to collect nanoparticles, proving that the synthetized IOMSNs have magnetic properties.

3.1.2 – Chemical Profile
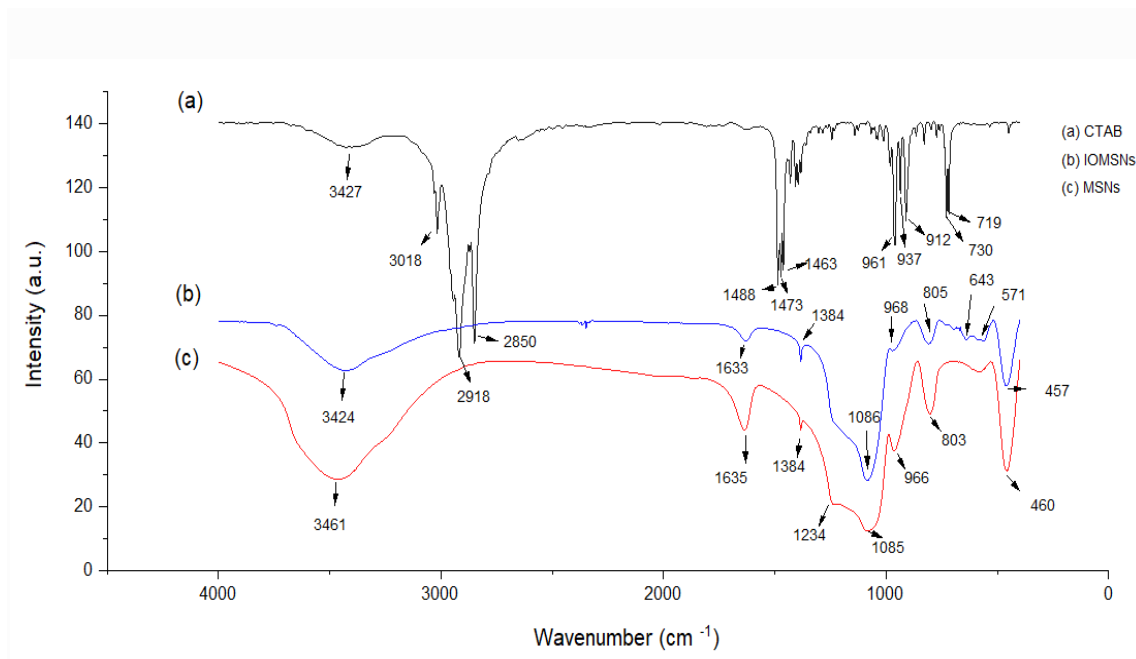
Figure 3.6 – FTIR analysis of CTAB, IOMSNs and MSNs.

A FTIR analysis was done to test if the surfactant template was removed during the sintering process that occurred at 540 ºC for 7 h (figure 3.5).

Typically, CTAB shows two intense peaks at 2800-3200 cm^{-1}, that correspond to the symmetric (2850 cm^{-1}) (80) and asymmetric (2918 cm^{-1}) stretching vibrations of the methylene chains (81). The 1488 cm^{-1} peak is attributed to the anti-symmetric angular vibration of CH_3– (N+) and the 1473 cm^{-1} is caused by the scissoring vibration of CH_2–(N+). C-C stretching vibrations can be found at 719-730 cm^{-1} (82).

Analysing MSNs FTIR spectrum and comparing it with CTAB, it is possible to conclude that the sintering at 540 ºC efficiently removed the surfactant template, since there is no similarity between the two spectra. Even so, it is possible to identify the main peaks corresponding to silica. The Si-O rocking vibration and Si-O bond stretching of surface Si-OH groups are shown at 460 cm^{-1} and 966 cm^{-1} respectively (83). The hydroxyl stretching band for both silanol Si-O-H and the water hydroxyls is at 3461 cm^{-1} in addition to the H-OH water twisting band at 1635 cm^{-1}. The internal Si-O-Si appear at 1085 cm^{-1} while the symmetric one at 803 cm^{-1} (81, 84).

Comparing the FTIR spectrum corresponding to MSNs with the IOMSNs one, it is possible to conclude that the silica coating is present in the IOMSNs. However, it was expected to find peaks related to the presence of iron in the sample, namely, peaks corresponding to the Fe-O (579 cm^{-1}) and Fe-O-Si (947 cm^{-1}) stretches (85) and they were not detected by FTIR analysis. The absence of Fe chemical bounds could be explained with the results obtained in EDS analysis (table 3.2), more specifically, the lower amounts of iron detected in IOMSNs analysis. On the other hand, comparing the IOMSNs FTIR spectrum with the one corresponding to CTAB it is

possible to conclude that as it happened with MSNs, the surfactant template was also removed during calcination process at 540 ℃.
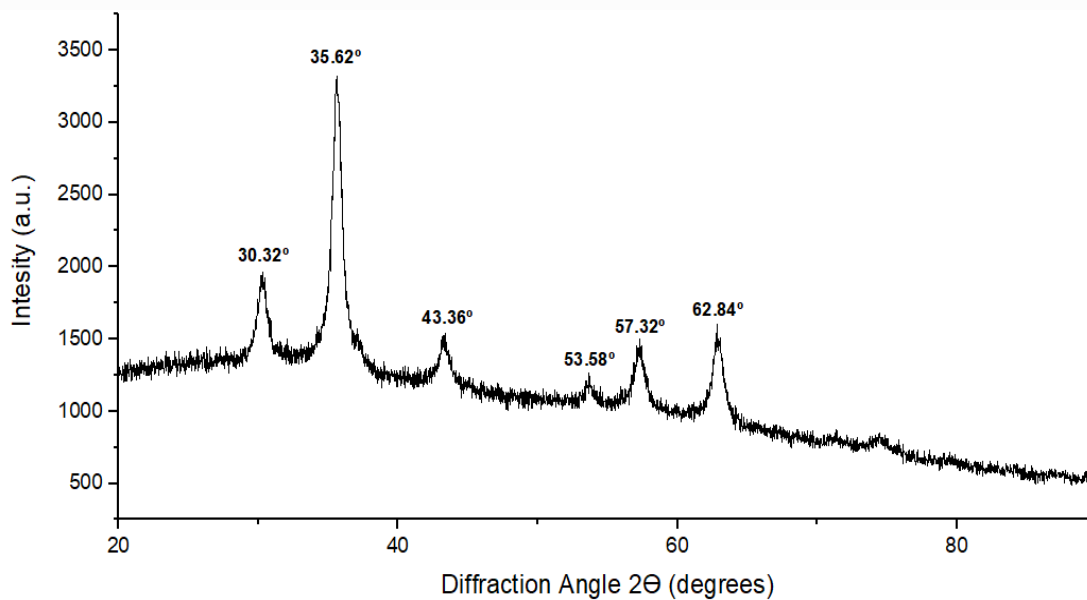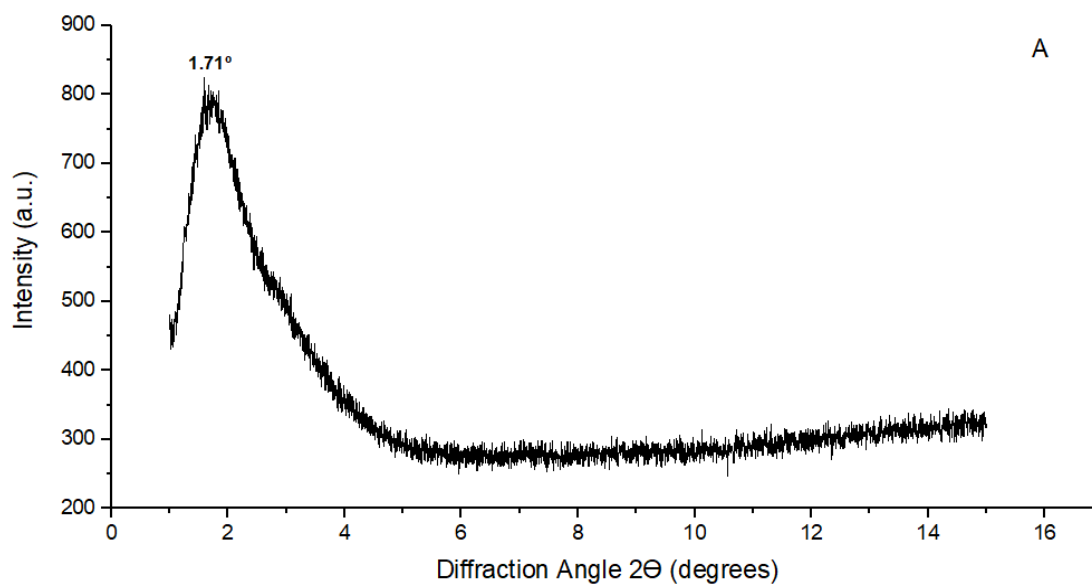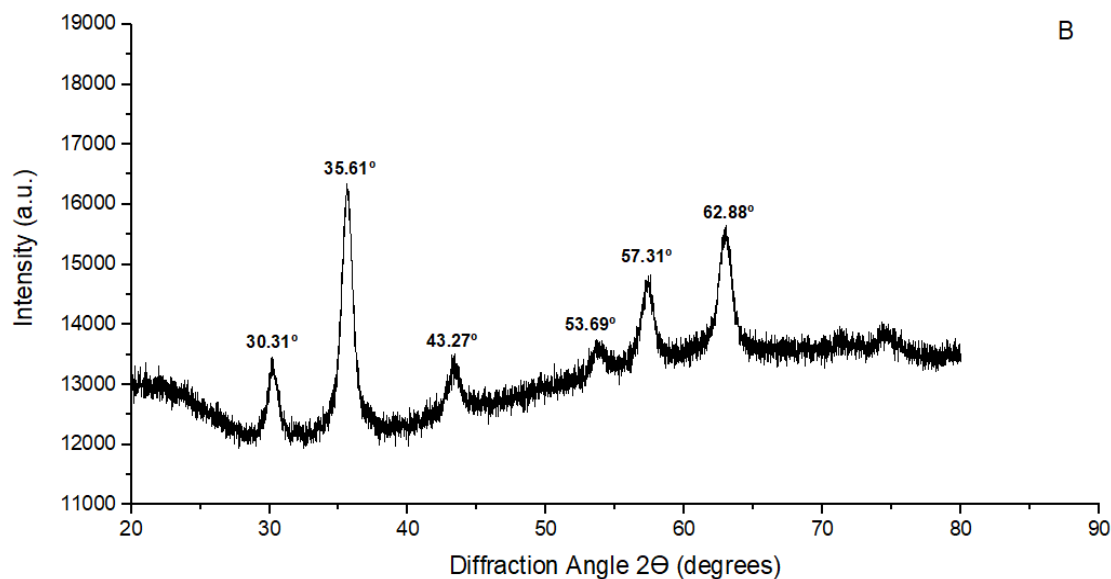
3.1.3 - Crystal phase analysis

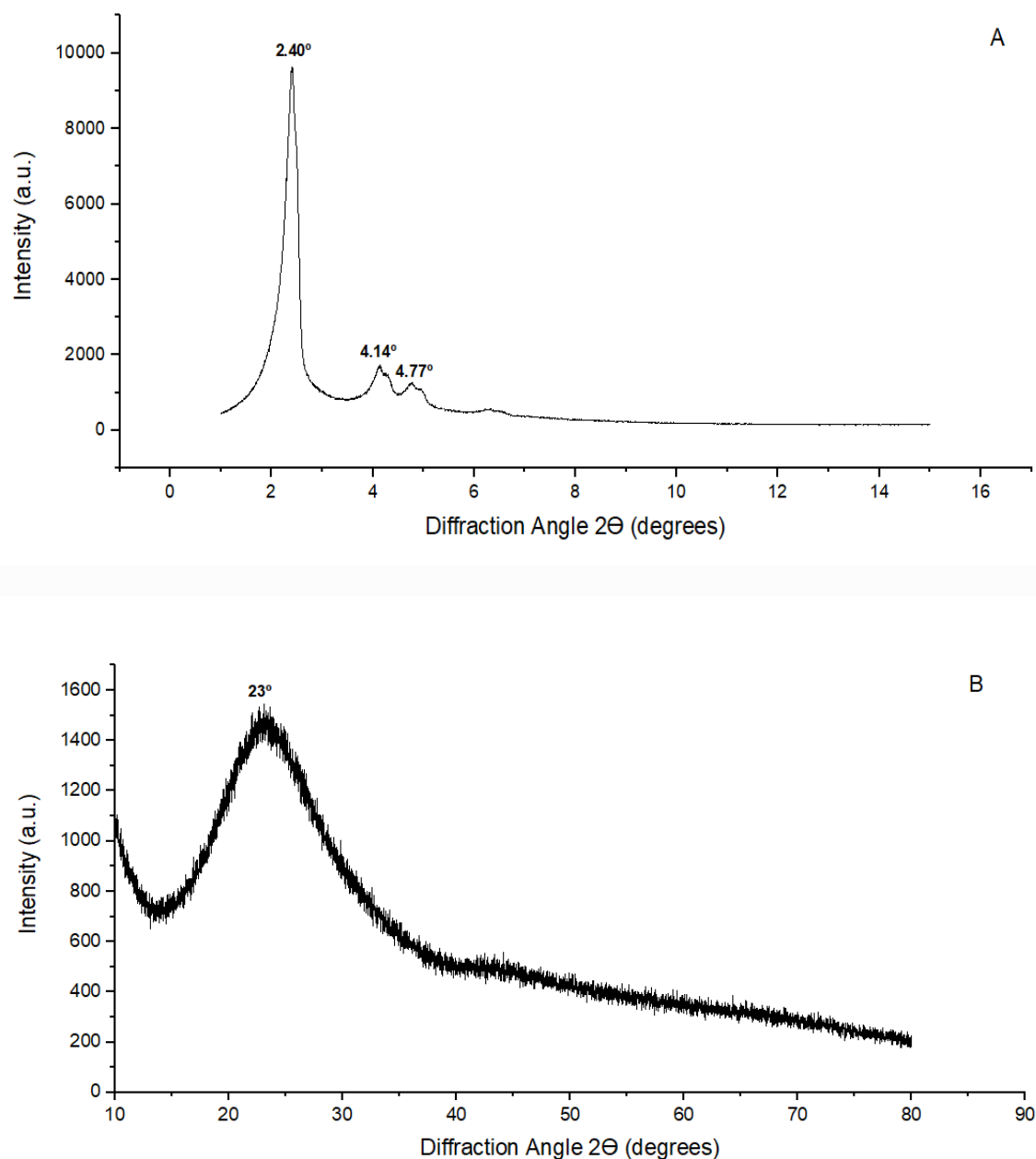**Figure 3.7** – XRD pattern of IONs.

Figure 3.8 – Low-angle XRD pattern of IOMSNs (A); Wide-angle XRD pattern of IOMSNs (B).

XRD analysis was performed to study the structure of IONs, IOMSNs and MSNs. The comparison of IONs XRD diffraction pattern with the one corresponding to IOMSNs, allowed to verify if during the calcination process, in which IOMSNs were summited to high temperatures (540 °C, 7 h), Fe_3O_4 (magnetite, which is the iron oxide that should be present in IOMSNs) was oxidised to γ-Fe_2O_3 (maghemite).

The X-Ray diffractogram of IONs exhibited reflections similar to the typical Bragg reflections of ferrites which are 30.1 °, 35.4 °, 43.1 °, 53.4 °, 56.9 °, 62.5 ° corresponding to the (220), (311), (400), (422), (511) and (440) planes, respectively. This features indicate that IONs are magnetite, with a crystalline structure, more specifically, with a cubic spinel structure (space group *Fd3m*) (86).

Analysing the LAXRD (Low-angle X-Ray Diffraction) pattern obtained for IOMSNs, it is possible do identify a strong diffraction peak at 2θ= 1.71 °, which can be attributed to the (100) Bragg reflection, characteristic of mesoporous with hexagonal symmetry of MCM-41-like materials (77).

In WAXRD (Wide Angle X-Ray diffraction) pattern, notorious peaks appear at 30.31 °, 35.61 °, 43.27 °, 53.69 °, 57.31 ° and 62.88 ° and they can be assigned to the (220), (311), (400), (422), (511), and (440) planes, showing that magnetite has an hexagonal phase structure (87). These results allow to conclude that magnetite was not oxidised into maghemite during the calcination process that occurred at 540 °C. Also, it is possible to conclude that silica has an amorphous structure, since there is a broad band peak between 20 ° and 30 °. It is possible to infer that both magnetite and silica are present in distinct phases, since the mesoporous silica coating has an amorphous phase, while magnetite, a crystalline one. These results are in agreement with previously reported studies regarding IOMSNs (88).

Figure 3.9 – Low-angle XRD pattern of MSNs (A); Wide-angle XRD pattern of MSNs (B).

The LAXRD (Low-angle X-Ray Diffraction) pattern obtained for MSNs is similar to the ones already described in the literature (89-92). Analysing it, it is possible to conclude that the synthesized MSNs exhibit reflections of 2.40 °, 4.14 ° and 4.77 ° that can be assigned to the lattice planes (100), (110) and (200) (93). These planes indicate a quasiregular arrangement of mesoporous with hexagonal symmetry, which is characteristic of MCM-41 type materials, that are mesoporous materials with a hierarchical structure from a family of silicates (90, 93). Analysing WAXRD (Wide-angle X-Ray Diffraction), there is a board band between 20 ° and 30 °, which corresponds to the amorphous silica (94-96) walls of solid MCM-41 (92).
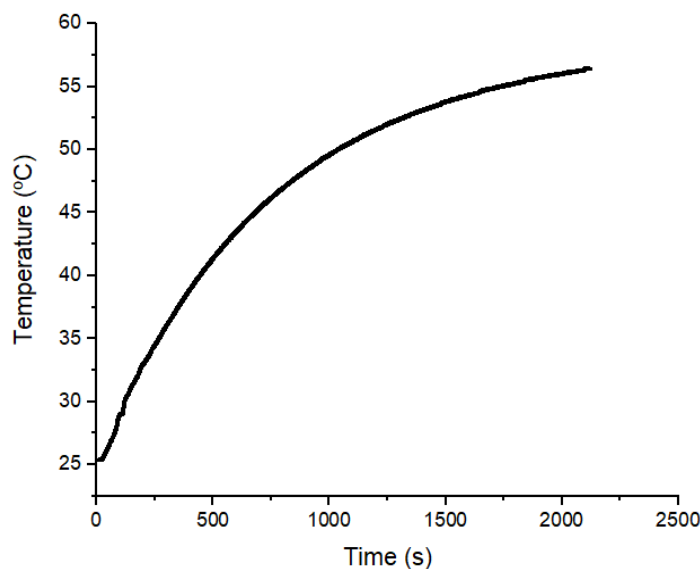
3.1.4 – Magnetic heating capacity: Hyperthermia

Figure 3.10 – Magnetic Heating Profile of IOMSNs.

The magnetic hyperthermia results obtained for IOMSNs are represented in figure 3.10. IOMSNs were dispersed in a 1% (m/V) solution of sodium citrate to obtain a stable solution, since nanoparticles have tendency to aggregate in aqueous media. Analysing the heating profile obtained for IOMSNs, it is possible to conclude that the sample's temperature increased approximately 56 °C in 35 minutes. A similar study was performed by Iqbal Y. *et al.* who analysed the magnetic heating capacity of silica coated iron oxide nanoparticles under an alternating magnetic field of 5.5 kA/m (approximately 69 Gauss) and 260 kHz, at different concentrations (3.5, 2.65, 2.2, 1.7, 1.3 and 0.9 mg/mL). They concluded that the saturation temperatures were achieved after approximately 600 seconds and they were 50 °C, 46 °C, 44 °C, 42 °C, 40 °C, and 38 °C, respectively. They also concluded that the optimum nanoparticles' concentration to achieve 42 °C, which is the temperature that induces cytotoxicity in cancer cells in hyperthermia, were obtained when the nanoparticles' concentration was 2.2 mg/mL. In this experiment, the IOMSNs concentration used was 7 mg/mL and comparing this concentration with the optimum nanoparticles' concentration tested in the study performed by Iqbal Y. *et al.*, it is possible to conclude that the IOMSNs synthesized in this experiment took more time (625 seconds) to achieve 42 °C even with a higher concentration and a stronger magnetic field, when compared to 2.2 mg/mL that was synthesized by Iqbal Y. *et al.* (600 seconds). It was expected that the synthesized IOMSNs reached the desired temperature (42 °C) more quickly than the particles at 2.2 mg/mL, since the magnetic heating capacity should increase with increasing nanoparticles concentration. However, it was not observed and there are two possible reasons to explain that. One might be related to the fact that the nanoparticles synthesized by Iqbal Y. *et al.* probably have a higher number of particles with iron in their constitution (97). And the other reason, may be due to the differences in nanoparticles' average

size, since the average size of IOMSNs is larger than that of the particles produced by Iqbal Y. *et al*. (97).

Besides that, the temperature of the synthesized IOMSNs should stabilize at 42 ℃ – higher temperatures are damaging for healthy cells around the tumour (98) - because it is known that if tumour region is maintained at this temperature for at least 30 minutes, cancer cells are destroyed (98). Although they have good magnetic heating capacity, IOMSNs did not stabilize at the required temperature. It was concluded that the synthesis protocol of IOMSNs should be optimized by increasing the amount of iron present, to have a better heating performance.
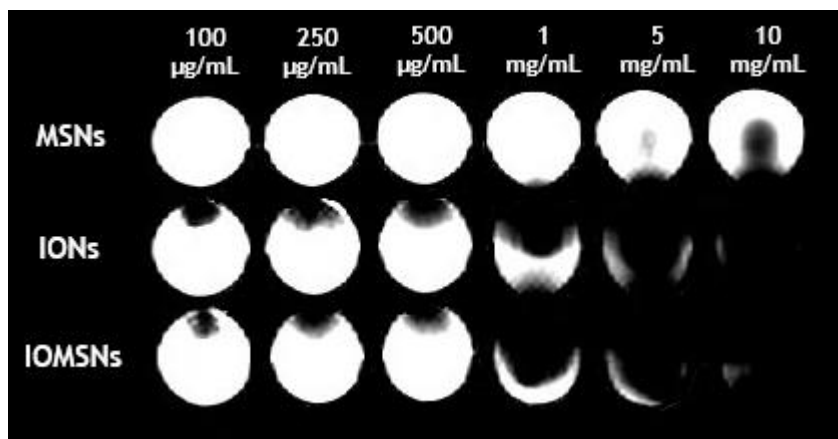
3.1.5 – Magnetic properties: Magnetic Resonance Imaging

Figure 3.11 – Magnetic Resonance Imaging of MSNs, IONs and IOMSNs, T2-weighted image.

Due to high soft tissue contrast, special resolution and penetration depth, Magnetic Resonance imaging (MRI) has become one of the most used and powerful tools for clinical diagnosis (99).

In order to improve the efficiency of diagnosis and allow a better distinction between healthy and unhealthy tissues, the research in medical imaging is being focused on the development of contrast agents (99, 100).

Magnetic nanoparticles have been extensively studied because of their potential to be used in medical diagnosis as MRI contrast agents. Their unique magnetic properties like magnetism, size and easy conjugation with biological functional units, are properties that make them ideal platforms for modifiable contrast agents in MRI. Their size and composition can be controlled in order to improve the magnetic parameters like saturation to magnetization which can change the MRI contrast (73).

There are several magnetic nanoparticles' systems under investigation, but their application *in vivo* is compromised due to toxic concerns. However, some superparamagnetic iron oxide nanoparticles (SPIONs) are already approved by FDA to be used as MRI contrast agents including Lumiren ® for bowel imaging, Feridex IV ® for spleen and liver imaging and Combidex ® for lymph node metastases imaging (99).

When a subject is placed under an external magnetic field, the magnetic moments of hydrogen atoms align with the field, producing an equilibrium magnetization along the z-axis (longitudinal magnetization). When the frequency of a radiofrequency pulse (RF) matches the precession frequency of the hydrogen protons, the magnetization vector rotates away from the z-axis to xy plan, in phase (transverse magnetization). Once the radiofrequency pulse is removed, the magnetization returns to equilibrium. The time necessary for this recovery is tissue-dependent (100).

MRI contrast is justified by differences in the proton density, spin-lattice relaxation time (T1) and spin-spin relaxation time (T2) of soft tissues. As it was explained in the previous sections, T1 is the time necessary for the magnetization vector return to equilibrium after a RF pulse. Protons with a short T1 recover rapidly the longitudinal magnetization and produce high signal intensities. On the other hand, for protons with a long T1, the full magnetization is not recovered after the application of subsequent RF pulses and so they produce low signal intensities. T2 is the time necessary to the exponential decay of transverse magnetization after a RF pulse. In T2-weighted images, protons with long T2 relaxation time produce high signal intensities while protons with short T2 relaxation time produce low signal intensities. In practice, the decay of transversal magnetization is not only caused by spin-spin interactions but also by the inhomogeneities in the main magnetic field. The combined relaxation time is described as T2* or effective T2 relaxation (99, 100).

To create MRI images, sequences of RF pulses are used. In each sequence, it is possible to vary the time between the beginning of the first pulse of a sequence and the first pulse of the next sequence - repetition time (TR). It is also possible to vary the time between the application of a RF pulse and the measurement of the correspondent MRI signal – echo time (TE). These two parameters also influence the contrast in MRI images (100).

Superparamagnetic iron oxide nanoparticles (SPIONs) act to alter T2 values of water protons around the particles. When placed under a magnetic field, the large magnetic moments of SPIONS align according to the field, creating heterogeneous field gradients. The coupling between the magnetic moments of SPIONs and the magnetic moments of the surrounding water protons cause efficient spin dephasing leading to a decrease of T2 relaxation time, producing low signal intensities in T2-weighted images. The contrast provided by SPIONs in MRI is called negative contrast since areas with high concentrations of SPIONs appear dark in T2-weighted images (99).

An MRI study was performed to determine the potential of IOMSNs to be used as a T2 contrast agent in MRI, using a 3 T clinical scanner (Sigma HDXT 3 T, GE Health Care, USA), with a TR= 2500 s, TE= 77.1 s and a FOV= 18.0x18.0 cm. For this purpose, Mesoporous silica nanoparticles (MSNs) and Iron Oxide nanoparticles (IONs) were used as controllers for this experiment. Since Mesoporous silica nanoparticles lack magnetic properties and cannot be used as MRI contrast agents, they were used as a negative control. IONs were used as positive control since, as previously mentioned, several contrast agents based on iron oxide nanoparticles were already approved by FDA to be used in MRI.

Analysing the results obtained (figure 3.11) it is possible to conclude that the signal intensities determined by IOMSNs are apparently similar to the ones obtained by IONs. This conclusion permits to infer that the mesoporous silica coating of IOMSNs does not seem to have influence on their performance in MRI. It is also possible to conclude that the signal intensity in the presented T2-weighted image decreased, with increasing nanoparticles concentration. These results are in accordance with the studies by Ali M.A *et al*. who proved the shortening T2

relaxation time effect of SPIONs and concluded that the increase in SPIONs concentration leads to a decrease in signal intensities in T2-weighted images (101).

The results obtained in this study may be an indicator that the synthesized IOMSNs have interesting characteristics to be used as MRI T2 contrast agents, once they produce signal intensities similar to those of IONs. Nevertheless, the commercialized products are based on superparamagnetic IONs and it is not known whether or not the synthesized IONs are superparamagnetic. Thus, it is necessary to perform complementary analyses such as Scanning SQUID microscopy, to determine the magnetization degree of IOMSNs in order to obtain a more accurate analysis of the results achieved.

In pursuance of a more reliable conclusion, it would be interesting to perform an MRI comparative study between the synthesized IOMSNs and a ION-based commercialized product (e.g. Feridex).

3.2 – Biological response
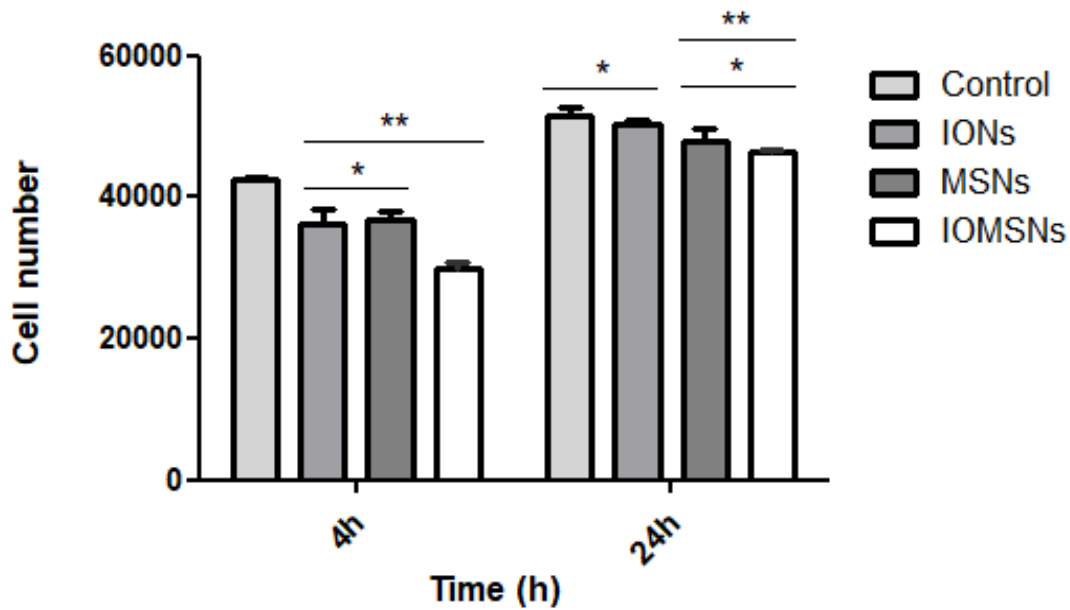
Figure 3.12 – Cell proliferation of HGnF after 4 and 24h of IONs, MSNs and IOMSNs at a concentration of 500 μg/mL (* indicates a significant statistical similarity; ** indicates a significant statistical difference from the control. ($p<0.05$)).
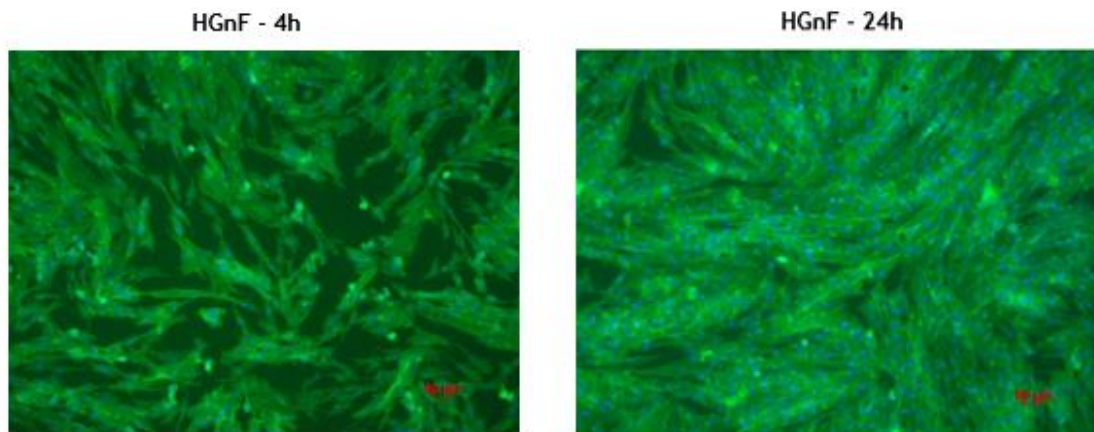
Figure 3.13 – Fluorescence Microscopy images HGnF cultured with IOMSNs after 4 h and 24 h. F-Actin is green and cells nuclei is blue. Scale bar: 50 μm. Magnification 100 x.

Nanoparticles' toxicity is a critical factor to consider when evaluating their potential to be used as a drug delivery system (102).

The aim of this study was to analyse the cytotoxic effect of IONs, MSNs and IOMSNs. For that purpose, two assays were performed, one to study the HGnF metabolic activity after 4 h

and 24 h of exposure to IOMSNs (Figure 3.12) and the other to verify if the cellular morphology changed with the introduction of IOMSNs in the cellular medium in the same time points (Figure 3.13). The choice of the cell line (HGnF), was due to the fact that tumour tissues are known to be surrounded by fibroblasts, which aid in malignant progression of tumour cells (103).

After 4 h, there was statistically relevant differences for all tested conditions comparing to the control, indicating that HGnF cultured with IONs, MSNs and IOMSNs had a different metabolic activity comparing to the HGnF cultured in control conditions. This was probably due to first cell-nanoparticle interaction, that cause a decrease in cell number. Comparing HGnF cultured with IONs and MSNs, statistical analysis demonstrated that the metabolic activity was similar for both types of nanoparticles.

After 24 h, there are no statistically relevant differences in cell number, between HGnF cultured with IONs and the HGnF cultured in control conditions, meaning that IONs are most likely to be non-cytotoxic for HGnF. Analysing the average size determined using DLS, it was expected that IONs induced cytotoxicity, due to their tendency to agglomerate. However, it did not happen, and it may be related to the fact that the cell-medium may increase the IONs dispersion. Nanoparticles' concentration may also influence cytotoxicity. Most of the studies regarding IONs revealed that they are cytotoxic for higher concentrations (>100 ug/mL) but it was also concluded that the toxicity dependents on different factors such as type of surface coating or its breakdown products, chemical composition of the cell-medium, oxidation state of iron and protein IONs interaction. Even so, the result obtained in this experiment is in agreement with a study performed by Chen J. *et al.*, who concluded that IONs did not present a significant decrease in cell viability for both SH-SY5Y (Human Neuroblastoma Cell line) and H4 (Human Neuroglioma cell line) after 48 h of incubation (104). A possible explanation for the similarity in cell viability between the cells cultured in control conditions and the cells cultured with IONs is due to iron oxide which is present in IONs. Iron is vital to health and for the development of bodily organs and several studies have shown that iron deficiency can be detrimental to cell cycle. Accordingly, the possible increasing availability of iron in the cellular medium may improve the condition of cell proliferation (105).

On the other hand, statistical analysis indicated that the cell growth was similar for both MSNs and IOMSNs. As cell viability of these types of nanoparticles was significantly different from the control, it is possible to conclude that they may induce some cytotoxicity, even in lower extension, since the cell number remains high for both types of nanoparticles after 24 h of incubation. The similarity in cell viability for MSNs and IONs can be explained by the fact that both types of nanoparticles have high amounts of silica in their constitution, even considering the lower amounts of iron oxide in IOMSNs. XRD results for MSNs and IOMSNs revealed the presence of silica with an amorphous structure and recent studies have been shown that amorphous silica may induce cytotoxicity against different types of cells, since it induces cell membrane damaged (106).

Comparing the cell proliferation of MSNs, IONs and IOMSNs, for both time points, it is concluded that IOMSNs, even presenting some cytotoxicity when compared to the control was the one that obtained a higher difference in the cell number between the two time points.

Analysing the fluorescence microscopy images obtained for HGnF cultured with IOMSNs (Figure 3.13) it is concluded that after 4 and 24 h of exposure to nanoparticles, the HGnF cells maintained their elongated morphology that is typical for this type of cells (107). In addition, fluorescence images also demonstrated the cell proliferation of HGnF in the presence of IOMSNs as their number clearly increase from 4 h to 24 h of culture.

Chapter 4

Conclusions and future perspectives

The main goal of this project was to combine the properties of magnetic nanoparticles and mesoporous silica nanoparticles to produce iron oxide mesoporous silica nanoparticles to work as nanocarriers for the drug delivery of Exemestane. For that purpose, three different types of nanoparticles, namely silica nanoparticles (SiNPs), mesoporous silica nanoparticles (MSNs) and iron oxide nanoparticles (IONs) were firstly synthesized and characterized as intermediate steps for the best understanding of the synthesis parameters that should be controlled during the synthesis of IOMSNs.

Regarding silica nanoparticles, it was proved that the synthesized particles have a good particle size (151 nm), a stable surface charge (-49.1 mV) and spherical morphology. The results obtained allow to conclude that the synthesized silica nanoparticles are suitable for biomedical applications due to their promising characteristics.

The synthesized mesoporous silica nanoparticles, have an average size of 197.4 nm and a rod-like morphology, however, the PDI value (0.381) indicates that they are polydisperse in solution, which is an indication of the presence of nanoparticles with random sizes. Regarding their surface charge, it was approximately -16.0 mV. This value should be closer to the surface charge obtained for silica nanoparticles and so it is concluded that MSNs should be optimized in order to have a higher stability in aqueous media. FTIR measurements confirmed that surfactant template was removed during the nanoparticles' calcination process at 540 ℃. Chrystal phase analysis showed that MSNs present a quasiregular arrangement of mesoporous with hexagonal symmetry and amorphous silica walls, characteristic of MCM-41 type materials.

Regarding iron oxide silica nanoparticles, it was demonstrated that nanoparticles are aggregated, which may be proved by the PDI value obtained (0.425). Regarding their surface charge, the value was approximately -16-6 mV and this value should be lower in order to increase the repulsion between the particles and consequently, increase their stability. Iron oxide nanoparticles were dispersed in sodium citrate, and a decrease in the average size was verified (182 nm) as well as the surface charge (-30.5 mV) which may indicate that citrates may be used in future approaches as stabilizer agents for iron oxide nanoparticles. Chrystal phase analysis also confirmed that the iron oxide present in IONs is magnetite, since its crystalline planes were identified in the IONs XRD pattern.

Iron oxide nanoparticles were obtained by combining the properties of mesoporous silica nanoparticles and iron oxide nanoparticles. The particles have an average size of approximately

469.6 nm and the PDI value obtained is higher (0.611), meaning that the particles have a random size distribution. Regarding surface charge, it was approximately -17.7 mV which reflects the lower repulsive forces between the particles. As well as for MSNs, IOMSNs were analysed using FTIR and the results also confirmed the elimination of CTAB during the calcination process. The presence of iron was tested using EDS-TEM and the results demonstrated that iron is present in IOMSNs even in lower atomic percentage when comparing to silica. Chrystal phase analysis using XRD demonstrated that IOMSNs assume a MCM-41-like hexagonal structure. It was also possible to identify the crystalline planes corresponding to magnetite, being possible to conclude that magnetite did not oxidise to maghemite during the IOMSNs calcination process. The XRD results allow to conclude that IOMSNs have silica in an amorphous phase and magnetite in a crystalline phase. The magnetic heating properties were also tested, no evaluate the potential of IOMSNs to be used as hyperthermia agents. The results demonstrated that IOMSNs have good heating capacity, however, the synthesis protocol should be optimized to enhance their potential to be used as a hyperthermia agent. It was also analysed the potential of IOMSNs to be used as magnetic resonance contrast agent and they demonstrated to have a great potential to be used as a T2 contrast agent. However, it is necessary to do an MRI comparative study with a ION-based commercialized product (e.g. Feridex).

To evaluate the biological response of human gingival fibroblasts to MSNs, IONs and IOMSNs, a resazurin assay were performed at two different time points, 4 h and 24 h. The results demonstrated that IOMSNs, even presenting some cytotoxicity when compared to the control conditions, was the one that obtained a higher difference in the cell number between 4 h and 24 h. Furthermore, fluorescence microscopy images obtained for HGnF cultured with IOMSNs allow to conclude that the cell morphology was not affected after 4 h and 24 h of exposure to IOMSNs, showing a good cell proliferation of HGnF (107).

Future perspectives

It will be necessary to test different alternatives to stabilize IONs. The next step is the optimization of the IOMSNs synthesis by controlling the molar ratio of TEOS and TEA, to obtain monodisperse iron oxide mesoporous silica nanoparticles with controllable sizes. It is also necessary to increase the amount of iron oxide (magnetite) used in the synthesis protocol of IOMSNs to obtain enhanced magnetic heating capacities.

Then, it will be necessary to do a SQUID analysis to study the magnetization of the particles.

The porosity must also be controlled to have a system that can work a possible nanocarrier for the drug delivery of Exemestane.

IOMSNs should be functionalized in order predict a good therapeutic performance in vivo, by functionalizing the surface with a hydrophilic polymer like PEG and adsorbing other ligands with affinity to cancer cells such as folic acid.

Then, the cytotoxicity of IOMSNs should be tested in breast cells to verify if they are non-cytotoxic per se. The final step should be test the drug delivery of Exemestane in ER-positive

breast cancer cells in order to evaluate the therapeutic effect of the developed drug delivery system.

54

References

1.   Cancer: World Health Organization; 2017 [Available from: http://www.who.int/cancer/en/.
2.   Cancer Country Profiles. World Health Organization 2014.
3.   Risk factors for cancer: National Cancer Institute; [updated December 23, 2015. Available from: https://www.cancer.gov/about-cancer/causes-prevention/risk.
4.   Cancer Prevention: World Health Organization; 2017 [cited 2017. Available from: http://www.who.int/cancer/prevention/en/.
5.   Global Cancer Facts and Figures. World Health Organization; 2015.
6.   Mechanisms of Carcinogenesis 3: World Health Organization - International Agency of Cancer Research; 2008 [Available from: https://www.iarc.fr/en/publications/pdfs-online/wcr/2008/wcr_2008_5.pdf.
7.   Weinberg RA. The biology of Cancer. 2nd ed2014.
8.   What is Cancer? 2017 [updated February 9, 2015.
9.   Geoffrey M. Cooper REH. The Cell. 4th ed. Washington, U.S.A: The American Society of Microbiology; 2007.
10.   Steichen SD, Caldorera-Moore M, Peppas NA. A review of current nanoparticle and targeting moieties for the delivery of cancer therapeutics. European Journal of Pharmaceutical Sciences. 2013;48(3):416-27.
11.   Akhter MH, Rizwanullah M, Ahmad J, Ahsan MJ, Mujtaba MA, Amin S. Nanocarriers in advanced drug targeting: setting novel paradigm in cancer therapeutics. Artificial cells, nanomedicine, and biotechnology. 2017:1-12.
12.   Shah TA, Guraya SS. Breast cancer screening programs: Review of merits, demerits, and recent recommendations practiced across the world. Journal of Microscopy and Ultrastructure. 2017;5(2):59-69.
13.   Coleman C, editor Early Detection and Screening for Breast Cancer. Seminars in Oncology Nursing; 2017: Elsevier.
14.   Sun T, Zhang YS, Pang B, Hyun DC, Yang M, Xia Y. Engineered nanoparticles for drug delivery in cancer therapy. Angewandte Chemie International Edition. 2014;53(46):12320-64.
15.   Lal S, Reed AEM, de Luca XM, Simpson PT. Molecular signatures in breast cancer. Methods. 2017.
16.   Chetlen A, Mack J, Chan T. Breast cancer screening controversies: who, when, why, and how? Clinical imaging. 2016;40(2):279-82.
17.   Klevos GA, Ezuddin NS, Vinyard A, Ghaddar T, Gort T, Almuna A, et al. A Breast Cancer Review: Through the Eyes of the Doctor, Nurse, and Patient. Journal of Radiology Nursing. 2017;36(3):158-65.
18.   Breast Anathomy: National Breast Cancer Foundation, Inc; 2017 [cited 2017 November 10, 2017]. Available from: http://www.nationalbreastcancer.org/breast-anatomy.
19.   Richard L. Drake AWV, Adam W.L. Mitchell. Gray's Anathomy for Students. 2nd ed: Churchill Livingstone; 2015 February 11, 2009. 1192 p.
20.   Breast Cancer: American Cancer Society; [cited 2017. Available from: https://www.cancer.org/cancer/breast-cancer.html.
21.   DCIS — Ductal Carcinoma In Situ: breastcancer.org; 2018 [Available from: http://www.breastcancer.org/symptoms/types/dcis.
22.   IDC — Invasive Ductal Carcinoma: breastcancer.org; 2018 [Available from: http://www.breastcancer.org/symptoms/types/idc.
23.   Treating Breast Cancer: American Cancer Society; 2017 [Available from: https://www.cancer.org/cancer/breast-cancer/treatment.html.
24.   Surgery to remove breast cancer (lumpectomy): Cancer Research UK; 2017 [Available from: http://www.cancerresearchuk.org/about-cancer/breast-cancer/treatment/surgery/remove-just-area-cancer.

25.   Surgery to remove your breast (mastectomy): Cancer Research UK; 2017 [updated October 24, 2017. Available from: http://www.cancerresearchuk.org/about-cancer/breast-cancer/treatment/surgery/remove-whole-breast.
26.   Surgery to remove lymph nodes: Cancer Research, UK; 2017 [updated October 24, 2017. Available from: http://www.cancerresearchuk.org/about-cancer/breast-cancer/treatment/surgery/remove-lymph-nodes.
27.   Targeted Therapy for Breast Cancer: American Cancer Society; 2017 [updated October 16, 2017; cited 2017 December 12, 2017]. Available from: https://www.cancer.org/cancer/breast-cancer/treatment/targeted-therapy-for-breast-cancer.html.
28.   Hegyi G, Szigeti GP, Szász A. Hyperthermia versus oncothermia: cellular effects in complementary cancer therapy. Evidence-Based Complementary and Alternative Medicine. 2013;2013.
29.   Wust P, Hildebrandt B, Sreenivasa G, Rau B, Gellermann J, Riess H, et al. Hyperthermia in combined treatment of cancer. The lancet oncology. 2002;3(8):487-97.
30.   McNamara K, Tofail SA. Nanosystems: the use of nanoalloys, metallic, bimetallic, and magnetic nanoparticles in biomedical applications. Physical Chemistry Chemical Physics. 2015;17(42):27981-95.
31.   Poonia N, Lather V, Pandita D. Mesoporous silica nanoparticles: a smart nanosystem for management of breast cancer. Drug discovery today. 2017.
32.   Simpson E. Sources of estrogen and their importance. The Journal of steroid biochemistry and molecular biology. 2003;86(3-5):225-30.
33.   Hiscox S, Davies EL, Barrett-Lee P. Aromatase inhibitors in breast cancer. Maturitas. 2009;63(4):275-9.
34.   Buzdar A. Exemestane in advanced breast cancer. Anti-cancer drugs. 2000;11(8):609-16.
35.   Kumar A, Sawant K. Encapsulation of exemestane in polycaprolactone nanoparticles: optimization, characterization, and release kinetics. Cancer nanotechnology. 2013;4(4-5):57-71.
36.   Parveen S, Misra R, Sahoo SK. Nanoparticles: a boon to drug delivery, therapeutics, diagnostics and imaging. Nanomedicine: Nanotechnology, Biology and Medicine. 2012;8(2):147-66.
37.   Rizvi SA, Saleh AM. Applications of Nanoparticle Systems in Drug Delivery Technology. Saudi Pharmaceutical Journal. 2017.
38.   Moreira AF, Dias DR, Correia IJ. Stimuli-responsive mesoporous silica nanoparticles for cancer therapy: A review. Microporous and Mesoporous Materials. 2016;236:141-57.
39.   McNamara K, Tofail SA. Nanoparticles in biomedical applications. Advances in Physics: X. 2017;2(1):54-88.
40.   Mudshinge SR, Deore AB, Patil S, Bhalgat CM. Nanoparticles: emerging carriers for drug delivery. Saudi pharmaceutical journal. 2011;19(3):129-41.
41.   Singh R, Lillard JW. Nanoparticle-based targeted drug delivery. Experimental and molecular pathology. 2009;86(3):215-23.
42.   Estelrich J, Sánchez-Martín MJ, Busquets MA. Nanoparticles in magnetic resonance imaging: from simple to dual contrast agents. International journal of nanomedicine. 2015;10:1727.
43.   Hahn MA, Singh AK, Sharma P, Brown SC, Moudgil BM. Nanoparticles as contrast agents for in-vivo bioimaging: current status and future perspectives. Analytical and bioanalytical chemistry. 2011;399(1):3-27.
44.   Asl HM. Applications of Nanoparticles in Magnetic Resonance Imaging: A Comprehensive Review. Asian Journal of Pharmaceutics (AJP): Free full text articles from Asian J Pharm. 2017;11(01).
45.   Shetake NG, Balla MM, Kumar A, Pandey BN. Magnetic hyperthermia therapy: An emerging modality of cancer treatment in combination with radiotherapy. Journal of Radiation and Cancer Research. 2016;7(1):13.
46.   Mamaeva V, Sahlgren C, Lindén M. Mesoporous silica nanoparticles in medicine—recent advances. Advanced drug delivery reviews. 2013;65(5):689-702.
47.   Rosenholm JM, Sahlgren C, Lindén M. Towards multifunctional, targeted drug delivery systems using mesoporous silica nanoparticles–opportunities & challenges. Nanoscale. 2010;2(10):1870-83.

48.   Mekaru H, Lu J, Tamanoi F. Development of mesoporous silica-based nanoparticles with controlled release capability for cancer therapy. Advanced drug delivery reviews. 2015;95:40-9.

49.   Yin H, Liao L, Fang J. Enhanced permeability and retention (EPR) effect based tumor targeting: the concept, application and prospect. JSM Clin Oncol Res. 2014;2(1):1010.

50.   Gaumet M, Vargas A, Gurny R, Delie F. Nanoparticles for drug delivery: the need for precision in reporting particle size parameters. European journal of pharmaceutics and biopharmaceutics. 2008;69(1):1-9.

51.   Zhang Y-N, Poon W, Tavares AJ, McGilvray ID, Chan WC. Nanoparticle–liver interactions: cellular uptake and hepatobiliary elimination. Journal of Controlled Release. 2016;240:332-48.

52.   An Y, Chen M, Xue Q, Liu W. Preparation and self-assembly of carboxylic acid-functionalized silica. Journal of Colloid and Interface Science. 2007;311(2):507-13.

53.   Chen X, Sun H, Hu J, Han X, Liu H, Hu Y. Transferrin gated mesoporous silica nanoparticles for redox-responsive and targeted drug delivery. Colloids and Surfaces B: Biointerfaces. 2017;152:77-84.

54.   Moskvin M, Babič M, Reis S, Cruz MM, Ferreira LP, Carvalho MD, et al. Biological evaluation of surface-modified magnetic nanoparticles as a platform for colon cancer cell theranostics. Colloids and Surfaces B: Biointerfaces. 2018;161:35-41.

55.   Tian Z, Yu X, Ruan Z, Zhu M, Zhu Y, Hanagata N. Magnetic mesoporous silica nanoparticles coated with thermo-responsive copolymer for potential chemo-and magnetic hyperthermia therapy. Microporous and Mesoporous Materials. 2018;256:1-9.

56.   ENERGY DISPERSIVE X-RAY SPECTROSCOPY (EDS) [Available from: https://www.mee-inc.com/hamm/energy-dispersive-x-ray-spectroscopyeds/.

57.   Lim J, Yeap SP, Che HX, Low SC. Characterization of magnetic nanoparticle by dynamic light scattering. Nanoscale research letters. 2013;8(1):381.

58.   Bhattacharjee S. DLS and zeta potential–What they are and what they are not? Journal of Controlled Release. 2016;235:337-51.

59.   Anoopkumar-Dukie S, Carey J, Conere T, O'sullivan E, Van Pelt F, Allshire A. Resazurin assay of radiation response in cultured cells. The British journal of radiology. 2005;78(934):945-7.

60.   Souza T, Ciminelli V, Mohallem N, editors. A comparison of TEM and DLS methods to characterize size distribution of ceramic nanoparticles. Journal of Physics: Conference Series; 2016: IOP Publishing.

61.   Eaton P, Quaresma P, Soares C, Neves C, de Almeida M, Pereira E, et al. A direct comparison of experimental methods to measure dimensions of synthetic nanoparticles. Ultramicroscopy. 2017;182:179-90.

62.   Masarudin MJ, Cutts SM, Evison BJ, Phillips DR, Pigram PJ. Factors determining the stability, size distribution, and cellular accumulation of small, monodisperse chitosan nanoparticles as candidate vectors for anticancer drug delivery: application to the passive encapsulation of [14C]-doxorubicin. Nanotechnology, science and applications. 2015;8:67.

63.   Clogston JD, Patri AK. Zeta potential measurement. Characterization of nanoparticles intended for drug delivery: Springer; 2011. p. 63-70.

64.   Verma A, Stellacci F. Effect of surface properties on nanoparticle–cell interactions. Small. 2010;6(1):12-21.

65.   Salatin S, Maleki Dizaj S, Yari Khosroushahi A. Effect of the surface modification, size, and shape on cellular uptake of nanoparticles. Cell biology international. 2015;39(8):881-90.

66.   Zhao J, Lu H, Wong S, Lu M, Xiao P, Stenzel MH. Influence of nanoparticle shapes on cellular uptake of paclitaxel loaded nanoparticles in 2D and 3D cancer models. Polymer Chemistry. 2017;8(21):3317-26.

67.   Do Kim K, Kim HT. Formation of silica nanoparticles by hydrolysis of TEOS using a mixed semi-batch/batch method. Journal of sol-gel science and technology. 2002;25(3):183-9.

68.   Shin Y, Lee D, Lee K, Ahn KH, Kim B. Surface properties of silica nanoparticles modified with polymers for polymer nanocomposite applications. Journal of Industrial and Engineering Chemistry. 2008;14(4):515-9.

69.   Huang X, Li L, Liu T, Hao N, Liu H, Chen D, et al. The shape effect of mesoporous silica nanoparticles on biodistribution, clearance, and biocompatibility in vivo. ACS nano. 2011;5(7):5390-9.

70.   Tsai CP, Hung Y, Chou YH, Huang DM, Hsiao JK, Chang C, et al. High‐Contrast Paramagnetic Fluorescent Mesoporous Silica Nanorods as a Multifunctional Cell‐Imaging Probe. Small. 2008;4(2):186-91.

71.   Yoncheva K, Popova M, Szegedi A, Mihály J, Tzankov B, Lambov N, et al. Functionalized mesoporous silica nanoparticles for oral delivery of budesonide. Journal of Solid State Chemistry. 2014;211:154-61.

72.   Kharisov BI, Dias HR, Kharissova OV, Vázquez A, Pena Y, Gomez I. Solubilization, dispersion and stabilization of magnetic nanoparticles in water and non-aqueous solvents: recent trends. RSC Advances. 2014;4(85):45354-81.

73.   Gupta AK, Gupta M. Synthesis and surface engineering of iron oxide nanoparticles for biomedical applications. Biomaterials. 2005;26(18):3995-4021.

74.   Kotsmar C, Yoon KY, Yu H, Ryoo SY, Barth J, Shao S, et al. Stable citrate-coated iron oxide superparamagnetic nanoclusters at high salinity. Industrial & Engineering Chemistry Research. 2010;49(24):12435-43.

75.   Erdemoğlu M, Sarıkaya M. Effects of heavy metals and oxalate on the zeta potential of magnetite. Journal of colloid and interface science. 2006;300(2):795-804.

76.   Dan M, Scott DF, Hardy PA, Wydra RJ, Hilt JZ, Yokel RA, et al. Block copolymer cross-linked nanoassemblies improve particle stability and biocompatibility of superparamagnetic iron oxide nanoparticles. Pharmaceutical research. 2013;30(2):552-61.

77.   Pereira C, Alves C, Monteiro A, Magen C, Pereira A, Ibarra A, et al. Designing novel hybrid materials by one-pot co-condensation: from hydrophobic mesoporous silica nanoparticles to superamphiphobic cotton textiles. ACS applied materials & interfaces. 2011;3(7):2289-99.

78.   Möller K, Bein T. Talented mesoporous silica nanoparticles. Chemistry of Materials. 2016;29(1):371-88.

79.   Lv X, Zhang L, Xing F, Lin H. Controlled synthesis of monodispersed mesoporous silica nanoparticles: Particle size tuning and formation mechanism investigation. Microporous and Mesoporous Materials. 2016;225:238-44.

80.   Coates J. Interpretation of infrared spectra, a practical approach. Encyclopedia of analytical chemistry. 2000.

81.   Quan G, Pan X, Wang Z, Wu Q, Li G, Dian L, et al. Lactosaminated mesoporous silica nanoparticles for asialoglycoprotein receptor targeted anticancer drug delivery. Journal of nanobiotechnology. 2015;13(1):7.

82.   Lin C, Fan B, Zhang JX, Yang X, Zhang H. Study on lead ion wastewater treatment of self-assembled film. Desalination and Water Treatment. 2016;57(45):21627-33.

83.   Karakassides MA, Gournis D, Petridis D. An infrared reflectance study of Si–O vibrations in thermally treated alkali-saturated montmorillonites. Clay Minerals. 1999;34(3):429-.

84.   Launer PJ. Infrared analysis of organosilicon compounds: spectra-structure correlations. Silicone compounds register and review. 1987;100.

85.   Nowostawska M, Corr SA, Byrne SJ, Conroy J, Volkov Y, Gun'ko YK. Porphyrin-magnetite nanoconjugates for biological imaging. Journal of nanobiotechnology. 2011;9(1):13.

86.   Pereira C, Pereira AM, Rocha M, Freire C, Geraldes CF. Architectured design of superparamagnetic Fe 3 O 4 nanoparticles for application as MRI contrast agents: mastering size and magnetism for enhanced relaxivity. Journal of Materials Chemistry B. 2015;3(30):6261-73.

87.   Moorthy MS, Seo D-J, Song H-J, Park SS, Ha C-S. Magnetic mesoporous silica hybrid nanoparticles for highly selective boron adsorption. Journal of Materials Chemistry A. 2013;1(40):12485-96.

88.   Sun X, Bai X, Liu X, editors. Preparation and characterization of magnetic mesoporous silica nanoparticles with a core-shell structure. Strategic Technology (IFOST), 2013 8th International Forum on; 2013: IEEE.

89.   Golezani AS, Fateh AS, Mehrabi HA. Synthesis and characterization of silica mesoporous material produced by hydrothermal continues pH adjusting path way. Progress in Natural Science: Materials International. 2016;26(4):411-4.

90.   Yan Y, Fu J, Liu X, Wang T, Lu X. Acid-responsive intracellular doxorubicin release from click chemistry functionalized mesoporous silica nanoparticles. RSC Advances. 2015;5(39):30640-6.

91.   Chen B, Wang Z, Quan G, Peng X, Pan X, Wang R, et al. In vitro and in vivo evaluation of ordered mesoporous silica as a novel adsorbent in liquisolid formulation. International journal of nanomedicine. 2012;7:199.

92.   Tayebee R, Amini M, Akbari M, Aliakbari A. A novel inorganic–organic nanohybrid material H 4 SiW 12 O 40/pyridino-MCM-41 as efficient catalyst for the preparation of 1-

amidoalkyl-2-naphthols under solvent-free conditions. Dalton Transactions. 2015;44(20):9596-609.

93.	Wei N, Zou X, Huang H, Wang X, Ding W, Lu X. Preparation of Well – Ordered Mesoporous – Silica – Supported Ruthenium Nanoparticles for Highly Selective Reduction of Functionalized Nitroarenes through Transfer Hydrogenation. European Journal of Organic Chemistry. 2018;2018(2):209-14.

94.	Wang P, Du M, Zhang M, Zhu H, Bao S. The preparation of tubular heterostructures based on titanium dioxide and silica nanotubes and their photocatalytic activity. Dalton Transactions. 2014;43(4):1846-53.

95.	Chen X, Jiang J, Yan F, Tian S, Li K. A novel low temperature vapor phase hydrolysis method for the production of nano-structured silica materials using silicon tetrachloride. RSC Advances. 2014;4(17):8703-10.

96.	Ullah R, Deb BK, Mollah MYA. Synthesis and characterization of silica coated iron-oxide composites of different ratios. International Journal of Composite Materials. 2014;4(2):135-45.

97.	Iqbal Y, Bae H, Rhee I, Hong S. Intensive analysis of core–shell silica-coated iron-oxide nanoparticles for magnetic hyperthermia. Journal of Nanoscience and Nanotechnology. 2016;16(11):11862-7.

98.	Pankhurst QA, Connolly J, Jones S, Dobson J. Applications of magnetic nanoparticles in biomedicine. Journal of physics D: Applied physics. 2003;36(13):R167.

99.	Stephen ZR, Kievit FM, Zhang M. Magnetite nanoparticles for medical MR imaging. Materials today. 2011;14(7-8):330-8.

100.	Philips Medical Systems B, the Netherlands. Understanding MRI: an interactive guide to MRI principles and applications 2001.

101.	Ali LM, Marzola P, Nicolato E, Fiorini S, Heras Guillamón Mdl, Piñol R, et al. Polymer-coated superparamagnetic iron oxide nanoparticles as T2 contrast agent for MRI and their uptake in liver. Future Science OA. 2017(0):FSO235.

102.	Lewinski N, Colvin V, Drezek R. Cytotoxicity of nanoparticles. small. 2008;4(1):26-49.

103.	Menon N, Leong DT. Cytotoxic Effects of Phosphonate-Functionalized Mesoporous Silica Nanoparticles. ACS applied materials & interfaces. 2016;8(3):2416-22.

104.	Chen 1 J, Zhu 1 J, Cho H-H, Cui K, Li F, Zhou X, et al. Differential cytotoxicity of metal oxide nanoparticles. Journal of Experimental Nanoscience. 2008;3(4):321-8.

105.	Ghasempour S, Shokrgozar MA, Ghasempour R, Alipour M. Investigating the cytotoxicity of iron oxide nanoparticles in in vivo and in vitro studies. Experimental and Toxicologic Pathology. 2015;67(10):509-15.

106.	Chang J-S, Chang KLB, Hwang D-F, Kong Z-L. In vitro cytotoxicitiy of silica nanoparticles at high concentrations strongly depends on the metabolic activity type of the cell line. Environmental Science & Technology. 2007;41(6):2064-8.

107.	Tsugeno Y, Sato F, Muragaki Y, Kato Y. Cell culture of human gingival fibroblasts, oral cancer cells and mesothelioma cells with serum-free media, STK1 and STK2. Biomedical reports. 2014;2(5):644-8.